



# Altered cerebellum development and impaired motor coordination in mice lacking the *Btg1* gene: Involvement of cyclin D1



Manuela Ceccarelli<sup>a,1</sup>, Laura Micheli<sup>a,1</sup>, Giorgio D'Andrea<sup>a,1</sup>, Marco De Bardi<sup>b</sup>, Blanca Scheijen<sup>c</sup>, MariaTeresa Ciotti<sup>a</sup>, Luca Leonardi<sup>a</sup>, Siro Luvisetto<sup>a</sup>, Felice Tirone<sup>a,\*</sup>

<sup>a</sup> Institute of Cell Biology and Neurobiology, National Research Council, Fondazione Santa Lucia, Rome, Italy

<sup>b</sup> Neuroimmunology and Flow Cytometry Unit, Fondazione Santa Lucia, 00143 Rome, Italy

<sup>c</sup> Laboratory of Pediatric Oncology, Radboud University Medical Centre, 6500 HB, Nijmegen, The Netherlands

## ARTICLE INFO

### Article history:

Received 5 August 2015

Received in revised form

3 October 2015

Accepted 4 October 2015

Available online 31 October 2015

### Keywords:

Postnatal neurogenesis  
Cerebellar precursor cells  
Neural cell proliferation  
Neural cell migration  
Cyclins

## ABSTRACT

Cerebellar granule neurons develop postnatally from cerebellar granule precursors (GCPs), which are located in the external granule layer (EGL) where they massively proliferate. Thereafter, GCPs become postmitotic, migrate inward to form the internal granule layer (IGL), further differentiate and form synapses with Purkinje cell dendrites.

We previously showed that the *Btg* family gene, *Tis21/Btg2*, is required for normal GCP migration. Here we investigated the role in cerebellar development of the related gene, *Btg1*, which regulates stem cell quiescence in adult neurogenic niches, and is expressed in the cerebellum.

Knockout of *Btg1* in mice caused a major increase of the proliferation of the GCPs in the EGL, whose thickness increased, remaining hyperplastic even after postnatal day 14, when the EGL is normally reduced to a few GCP layers. This was accompanied by a slight decrease of differentiation and migration of the GCPs and increase of apoptosis. The GCPs of double *Btg1/Tis21*-null mice presented combined major defects of proliferation and migration outside the EGL, indicating that each gene plays unique and crucial roles in cerebellar development. Remarkably, these developmental defects lead to a permanent increase of the adult cerebellar volume in *Btg1*-null and double mutant mice, and to impairment in all mutants, including *Tis21*-null, of the cerebellum-dependent motor coordination. Gain- and loss-of-function strategies in a GCP cell line revealed that *Btg1* regulates the proliferation of GCPs selectively through cyclin D1. Thus, *Btg1* plays a critical role for cerebellar maturation and function.

© 2015 Elsevier Inc. All rights reserved.

## 1. Introduction

The cerebellum is required for motor coordination and learning, and is implicated in cognition and emotion as well as in related pathologies such as autism (Reeber et al., 2013). Thus, elucidating the mechanisms controlling the generation of the cerebellar neurons is critical to understand these processes and their pathologies.

During mid gestation, a subset of progenitor cells in the brain ventricular zone migrates to the rhombic lip, germinative epithelium located at the roofplate of the fourth ventricle, where they are specified to the neural lineage under the influence of bone morphogenetic proteins and of the transcription factor *Math1* (Alder et al., 1996, 1999; Ben-Arie et al., 1997; Wang and Wechsler-Reya, 2014). These progenitors migrate from the upper rhombic lip over the surface of the cerebellar anlage to form the external granule layer (EGL) of cerebellar primordia, where they become precursor cells of the cerebellar granule neurons (GCPs; Wingate, 2001). In the EGL the GCPs continue to proliferate actively, in the mouse until the second postnatal week, under the influence of Sonic Hedgehog, secreted by the Purkinje cells (Dahmane and Ruiz i Altaba, 1999; Wallace, 1999; Wechsler-Reya and Scott, 1999).

Finally, GCPs exit the cell cycle and migrate inward to the cerebellar internal granule layer (IGL) below the Purkinje cell soma, differentiating into mature granule neurons (Fujita et al., 1966; Rakic, 1971). The signals triggering these processes are poorly

\* Correspondence to: Institute of Cell Biology and Neurobiology, Consiglio Nazionale delle Ricerche, Fondazione S.Lucia, via del Fosso di Fiorano 64, 00143 Rome, Italy.

E-mail addresses: [manu.ceccarelli@gmail.com](mailto:manu.ceccarelli@gmail.com) (M. Ceccarelli), [laura.micheli@cnr.it](mailto:laura.micheli@cnr.it) (L. Micheli), [dandrea.giorgio@gmail.com](mailto:dandrea.giorgio@gmail.com) (G. D'Andrea), [m.debardi@hsantalucia.it](mailto:m.debardi@hsantalucia.it) (M. De Bardi), [Blanca.Scheijen@radboudumc.nl](mailto:Blanca.Scheijen@radboudumc.nl) (B. Scheijen), [mariaTeresa.ciotti@cnr.it](mailto:mariaTeresa.ciotti@cnr.it) (M. Ciotti), [luca.leonardi@cnr.it](mailto:luca.leonardi@cnr.it) (L. Leonardi), [siro.luvisetto@cnr.it](mailto:siro.luvisetto@cnr.it) (S. Luvisetto), [felice.tirone@cnr.it](mailto:felice.tirone@cnr.it) (F. Tirone).

<sup>1</sup> These authors have contributed equally.

understood. They play a key role not only in the normal development of the cerebellum, but also, when a misregulation occurs, in the formation of medulloblastoma, a most common childhood tumor arising in 20% of cases from GCPs (Kadin et al., 1970; Marino, 2005; Schüller et al., 2008; Yang et al., 2008; Gibson et al., 2010).

In this context, we have recently provided evidence for the role played as a medulloblastoma suppressor by the antiproliferative and prodifferentiative gene *Tis21/Btg2* (also known as PC3, hereafter referred to as *Tis21*; Bradbury et al., 1991; Rouault et al., 1996). Overexpression of this gene inhibits the proliferation of normal and neoplastic GCPs and facilitates their differentiation (Farioli-Vecchioli et al., 2007). Surprisingly, however, when *Tis21* is ablated, in cerebellum the proliferation of GCPs does not change, but their migration is strongly inhibited in consequence of the decrease of the chemokine *Cxcl3* within the GCPs. This defect of migration causes a longer exposure of GCPs to *Shh* and a great increase of medulloblastoma frequency (Farioli-Vecchioli et al., 2012a,b).

Given the antiproliferative action of *Tis21* in several neural and non-neural tissues (Boiko et al., 2006; Evangelisti et al., 2009; Montagnoli et al., 1996; Farioli-Vecchioli et al., 2009, 2014a), a question arising from these findings is whether *Tis21*-null GCPs do not increase their proliferative rate because other genes substitute for the absence of *Tis21*. Among these may be the *Tis21* family-related gene *Btg1*, which is expressed in several neural tissues including cerebellum, and also in the subventricular zone and dentate gyrus, where it inhibits the proliferation of adult neural stem cells and controls their self-renewal (Farioli-Vecchioli et al., 2012c). It is known that *Btg1* inhibits cellular proliferation (Rouault et al., 1992; Li et al., 2009; Zhu et al., 2013) by regulating the S-phase of the cell cycle (Farioli-Vecchioli et al., 2014b).

We therefore analyzed the functional role of *Btg1* in the proliferation, differentiation and migration of GCPs and its role in cell cycle control. We found that *Btg1* is required to negatively control the proliferation of GCPs and, to a lesser extent, their differentiation; furthermore, *Btg1* controls the G1 to S phase transition by quite selectively regulating cyclin D1 expression. By using double mutant *Btg1/Tis21*-null mice we revealed the specific requirement of *Btg1* to control the proliferation of the GCPs, whereas their migration was essentially dependent on *Tis21*. Furthermore, the developmental defects arising from the ablation of *Btg1* alone or with *Tis21* result in permanent deficits of motor coordination, thus highlighting the importance of *Btg1* in the normal development and function of the cerebellum.

## 2. Materials and methods

### 2.1. Mouse lines and genotyping

The *Btg1* knockout mouse line was previously generated in the C57BL/6 strain as described (Farioli-Vecchioli et al., 2012c), by inserting the neomycin resistance cassette within exon I of the *Btg1* gene. Genotyping of mice was routinely performed by PCR analysis, using genomic DNA from tail tips as described (Farioli-Vecchioli et al., 2012c). The *Tis21* knockout mouse line was previously generated and described (Farioli-Vecchioli et al., 2009). The double mutant *Btg1<sup>-/-</sup>/Tis21<sup>-/-</sup>* mice and the *Btg1<sup>+/+</sup>/Tis21<sup>+/+</sup>*, *Btg1<sup>-/-</sup>/Tis21<sup>+/+</sup>*, *Btg1<sup>+/+</sup>/Tis21<sup>-/-</sup>* mice (referred throughout this report to as wild-type, *Btg1<sup>-/-</sup>* and *Tis21<sup>-/-</sup>*, respectively) were generated by multiple intercrossing between *Btg1<sup>-/-</sup>* and *Tis21<sup>-/-</sup>* mice, until an isogenic progeny was obtained. *Math1*-green fluorescent protein mice (*Math1*-GFP) express GFP driven by the *Math1* enhancer (Lumpkin et al., 2003), and were crossed to the *Btg1<sup>-/-</sup>* mice to obtain GFP/*Btg1<sup>-/-</sup>* mice. Cerebellar

morphology and volumes were measured in male mice; the other experiments were performed with mice of both sexes, and all animal procedures were completed in accordance with the current European (directive 2010/63/EU) Ethical Committee guidelines. *Btg1* knockout mice are available upon request to J.-P. Rouault.

### 2.2. Bromodeoxyuridine treatment of mice and cell lines

GCPs entering S-phase were detected 1 h after an injection of bromodeoxyuridine (BrdU) (95 mg/kg, i.p.), according to existing protocols (Canzoniere et al., 2004; Qiu et al., 2010).

GCPs migrating from the EGL to the inner layers were visualized either 42 h or 5 days after a single injection of BrdU (95 mg/kg, i.p.) in P7 (postnatal day 7) and P14 mice.

BrdU incorporation in C17.2 cerebellar cells, in cyclin D1<sup>+/+</sup> and cyclin D1<sup>-/-</sup> mouse embryo fibroblasts (MEFs) and in DAOY medulloblastoma cells, was performed as previously described (Guardavaccaro et al., 2000), by adding 50 μM BrdU to exponentially growing cultures 18 h (or 24 h in MEFs) before fixation.

### 2.3. Immunohistochemistry: sample preparation, BrdU labeling, antibodies, and image analysis

Immunohistochemistry was performed on free-floating cerebellar sections, stained for multiple labeling and BrdU incorporation by fluorescent methods, as described (Canzoniere et al., 2004; Farioli-Vecchioli et al., 2007). Briefly, for EGL analysis, cerebella of P7 and P14 mice were dissected and fixed by overnight immersion in 4% PFA in PBS; cerebella of P60 mice were dissected after transcardiac perfusion with 4% PFA in PBS and kept overnight in PFA. Fixed cerebella were then equilibrated in 30% sucrose in PBS and cryopreserved at -80 °C until use. Cerebella were then embedded in Tissue-Tek OCT (Sakura Finetek, CA, USA) and cut at -25 °C in midsagittal sections of 40 μm. BrdU-labeled or cyclin-positive cells were detected in sections pretreated to denature the DNA, with 2 N HCl 45 min at 37 °C and then with 0.1 M sodium borate buffer, pH 8.5, for 10 min. The following primary antibodies were used: a rat monoclonal antibody against BrdU (AbD Serotec; MCA2060; 1:300), goat polyclonal antibodies against NeuroD1 (R&D Systems; AF2746; 1:100) or Calbindin (Santa Cruz Biotechnology, CA, USA; sc-7691; 1:100), a mouse monoclonal antibody raised against NeuN (Merck Millipore, MA, USA; MAB377; 1:100), or rabbit polyclonal antibodies against cleaved (activated) Caspase-3 (Cell Signaling Technology; 9661; 1:100) or GFAP (DakoCytomation, Denmark; Z0334; 1:250). Moreover, cyclins were detected in the EGL sections by using a rabbit monoclonal antibody against cyclin D1 (Merck Millipore; clone EP272Y; 1:50), or rabbit polyclonal antibodies against cyclin D2 (Santa Cruz; sc-593; 1:50) or cyclin A (Santa Cruz; sc-596; 1:50).

Images of the immunostained sections were captured by a confocal laser scanning TCS SP5 microscope (Leica Microsystems) and were analyzed by the I.A.S. software (Delta Sistemi, Rome, Italy).

### 2.4. Cell culture and cell lines

C17.2 cells—an immortalized line of cerebellar precursor cells (Ryder et al., 1990)—and cyclin D1<sup>+/+</sup> and cyclin D1<sup>-/-</sup> MEFs were cultured in DMEM (Guardavaccaro et al., 2000), while DAOY cells in Minimum Essential Medium (MEM), containing 10% fetal calf serum. All cell lines were kept in a humidified atmosphere of 5% CO<sub>2</sub> at 37 °C.

## 2.5. Immunofluorescence staining in cell lines

To visualize BrdU, Flag and  $\beta$ Gal in C17.2, DAOY cells and cyclin D1<sup>+/+</sup> and cyclin D1<sup>-/-</sup> MEFs, either the rat monoclonal antibody against BrdU indicated above (MCA2060), or the mouse monoclonal M2 antibody against Flag (Sigma Aldrich, St.Louis, MO, USA; F3165; 1:200), or a rabbit polyclonal antibody against  $\beta$ Gal (Merck Millipore; AB1211; 1:100), were used respectively. Anti-BrdU, anti-Flag and anti- $\beta$ Gal antibodies were visualized by donkey anti-rat TRITC-conjugated, donkey anti-mouse Alexa 488-conjugated, and by donkey anti-rabbit Alexa 488-conjugated secondary antibodies, respectively (Jackson ImmunoResearch).

In C17.2 cell cultures infected with either pSR-neo-GFP-shBtg1 or pSR-neo-GFP-shLUC, the green fluorescent protein was directly visualized by microscopy.

The images of the immunostained cells were obtained by an Olympus Optical (Tokyo, Japan) BX53 fluorescence microscope connected to a Spot RT3 camera (Diagnostic Instruments Inc, Sterling Heights, MI, USA).

## 2.6. Immunoblotting analysis and antibodies

We followed described procedures (Guardavaccaro et al., 2000). Briefly, transfected or infected C17.2 cell cultures were lysed into lysis buffer (50 mM Tris-HCl [pH 7.4], 150 mM NaCl, 1 mM EDTA, 10% glycerol, 1% NP40) containing 1 mM phenylmethylsulfonyl fluoride (PMSF), 10  $\mu$ g per ml of leupeptin and aprotinin, 10 mM  $\beta$ -glycerophosphate, 4 mM NaF, 0.1 mM Na<sub>3</sub>VO<sub>4</sub>, and sonicated. Proteins were electrophoretically analyzed by SDS-12% PAGE and transferred to nitrocellulose membranes; these were incubated with the indicated antibodies for 2 h in blocking buffer (TBS [10 mM Tris HCl (pH 8), 150 mM NaCl]-0.05% Tween-5% powdered milk) and then incubated in the same buffer for 2 h with the primary antibody.

The antibodies used for immunoblots were: the affinity-purified rabbit polyclonal antibodies anti-cyclin A (sc-596), anti-cyclin E (sc-481), anti-cyclin D2 (Santa Cruz; sc-593; 1:200) and anti-cyclin B1 (sc-595), the mouse monoclonal antibodies anti-cyclin D1 72-13G specific for rodent cyclin D1 and anti-cyclin B1 (sc-245; used in experiments of overexpression of Btg1), all from Santa Cruz Biotechnology (diluted 1:200); the mouse monoclonal antibodies anti-Flag M2 (Sigma Aldrich, 1:400), or DM1A anti- $\alpha$ -Tubulin (Sigma Aldrich T6199; 1:10.000).

## 2.7. Quantification of cell numbers and thickness in EGL

The proliferating, differentiating, apoptotic and cyclin-positive cells in the EGL at P7 or P14 were measured on at least five non-adjacent midsagittal sections per mouse at the midpoint of the fifth, seventh, and ninth folia of each section, according to published protocols (Farioli-Vecchioli et al., 2012a; Kokubo et al., 2009); three mice for each genotype were analyzed. In the same sections the EGL thickness was measured, calculated by measuring the distance between the pial surface and the beginning of the ML. Purkinje cells, identified as Calbindin-positive in P60 cerebella, were counted on one-in-six cerebellar sections at the midpoint of the fifth, seventh, and ninth folia; at least three mice for each genotype were analyzed.

## 2.8. Cell migration assays in vivo, layer areas and volumes

The GCPs migrating from the EGL were identified as BrdU-labeled cells in each defined layer (i.e., EGL, ML, or IGL) and were counted as percentage ratio to the total number of BrdU-labeled cells in all three layers, in five nonadjacent midsagittal sections at the midpoint of the fifth, seventh, and ninth folia. Three mice per

genotype were analyzed. For planimetric and volume measurements we followed our published procedure (Farioli-Vecchioli et al., 2012a). Briefly, planimetric measurements of the cerebellar area (or of layers) were carried out throughout the whole extension of the cerebellum in one-in-six series of sagittal sections and for the whole length of the cerebellar cortex (or of the layer) in each photomicrograph field (5 $\times$ ), by tracing the outline of the area on a digital picture analyzed using the I.A.S. software (Delta Sistemi). The volume of the cerebellum was calculated multiplying the average cerebellar area by section thickness and by number of sections.

### 2.8.1. Isolation of cerebellar granule progenitor cells from the EGL and in vitro migration assay

We analyzed the migration of GFP<sup>+</sup> GCPs, purified from GFP/Btg1<sup>+/+</sup> and GFP/Btg1<sup>-/-</sup> P7 mice, through poly-D-lysine-coated membranes with 8  $\mu$ m pore size (0.3 cm<sup>2</sup>) in a modified Boyden chamber, as previously described (Lu et al., 2001; Farioli-Vecchioli et al., 2012a). Isolation of GCPs was as described in Farioli-Vecchioli et al. (2012a) and separated by fluorescence-activated cell sorting (FACS) on a MoFlo high-speed cell sorter (Beckman Coulter).

## 2.9. Behavioral assessments of motor functions

Mice, at the age of 2 months (P60), were tested in the rotarod test and in the horizontal bar test to assess their motor coordination, balance and neuromuscular strength, as described (Marazziti et al., 2013).

### 2.9.1. Rotarod test

In this test, used to assess motor coordination and balance, mice had to keep their balance on a rotating rod (3-cm diameter) set at an accelerating speed from 4 to 40 rpm in 300 s (model 47600; Ugo Basile). To familiarize themselves with the apparatus, mice underwent a training session of three trials, 60 s each, in which the rod was kept stationary for the first trial and held at 4 rpm for the last two trials. The next day, and the 3 following days, mice were tested to evaluate motor learning (three trials per day with an intertrial interval of at least 30 min). The latency to fall from the rotating rod was recorded in each trial. Data for each of the 4 consecutive days is reported as the average of the three daily trials ( $\pm$  SEM).

### 2.9.2. Horizontal bar test

The horizontal bar test was performed to evaluate the neuromuscular strength. This test is based on the latency of a mouse to fall off from a thin metallic bar, where it is clinging with its forepaws. To perform this test, mice were held so that they cling with their forelimbs to a thin metallic bar (25 cm long-2-mm thick) extended between two poles 30 cm high. Time spent on the bar was registered for up to 180 s. Three trials with an intertrial interval of at least 30 min were considered. Data is reported as the average ( $\pm$  SEM) of three trials.

## 2.10. Btg1 expression vectors and plasmids

The Btg1 expression vector pSCT-HA-FLAG-Btg1 was constructed by cloning in the NotI site of the vector pSCT (see Guardavaccaro et al., 2000) the synthesized coding region of the mouse Btg1 cDNA (nucleotides 325–840), followed by 2xHA and FLAG sequences. A pSCT-Btg1 construct, generated by cloning in BamHI-5' XbaI-3' of the pSCT vector the Btg1 coding sequence amplified by PCR, was used to check that the HA-FLAG peptide did not interfere with the biological activity of the Btg1 protein. These constructs were confirmed by sequencing. The pSCT- $\beta$ Galactosidase (pSCT- $\beta$ Gal) vector

and the cyclins vectors have been previously described (Guardavaccaro et al., 2000).

### 2.10.1. Design of siRNA targeting *Btg1*; generation of shRNA recombinant virus and infection

The 19-nucleotide siRNA sequences specific to mouse *Btg1* and cyclin D1 mRNAs or to luciferase were designed with the on-line Design Tool software (MWG, Ebersberg, Germany). The best candidate sequence was used to synthesize a pair of 64-mer oligonucleotides that were cloned in the BglIII-5' HindIII-3' sites of the retroviral expression vectors pSUPER.retro-neo-GFP (sh*Btg1* and shLUC) or pSUPER.retro-puro (shcyclin D1), according to the manufacturer's instructions (Oligoengine, Inc., Seattle). The siRNA *Btg1*-421 sequence was as follows: 5'-ATGGTAGACAGCAGAATCA-3', while the siRNA cyclin D1-416 sequence was: 5'-TGGAACGCTTCTGGTGAA-3'. The control sequence from the luciferase gene was 5'-ACGGATTACCAGGGATTTC-3'; the vector pSUPER.retro-puro-LUC had been previously generated (Micheli et al., 2011). The presence of the correct sequence cloned in pSUPER.retro-neo-GFP or in pSUPER.retro-puro was confirmed by sequencing.

Retroviruses from the pSUPER.retro-neo-GFP-sh*Btg1*-421 and pSUPER.retro-neo-shLUC, or pSUPER.retro-puro-shcycD1-416 and pSUPER.retro-puro-LUC constructs were generated by transfecting them into the packaging Phoenix helper cells using Lipofectamine (Life Technologies, Carlsbad, CA, USA) and used for infection of C17.2 cells as previously described (Micheli et al., 2011); selection of cell cultures infected with viruses carrying puromycin resistance (shcycD1 and shLUC vectors) was applied for 5 days.

### 2.11. RNA extraction, real-time RT-PCR

Total cellular RNA was extracted from C17.2 cells using Trizol reagent (Invitrogen, San Diego, CA, USA) following the manufacturer's instructions and reverse-transcribed and analyzed by real-time PCR as previously described (Farioli-Vecchioli et al., 2012a).

## 3. Results

### 3.1. Postnatal developmental alterations in *Btg1*<sup>-/-</sup>, *Tis21*<sup>-/-</sup> and *Btg1*<sup>-/-</sup>/*Tis21*<sup>-/-</sup> cerebella

First we analyzed whether the genetic ablation of *Btg1* affected the proliferation of GCPs in the EGL at P7 and P14. These stages correspond to the age of highest expansion of GCPs, and to the end of their proliferative development in the EGL, respectively.

At P7 the percentage of proliferating GCPs, located in the outer region of the EGL and identified by incorporation of BrdU after 1 h pulse, increased significantly in *Btg1* knockout mice (about 22%, compared with control mice (Fig. 1A,B; *Btg1*<sup>-/-</sup> vs *Btg1*<sup>+/+</sup>,  $p < 0.00001$ ). An even larger increase of proliferation was detected in *Btg1* knockout mice at P14, relative to control mice (35% increase; Fig. 1A,B; *Btg1*<sup>-/-</sup> vs *Btg1*<sup>+/+</sup>,  $p < 0.00001$ ). In addition, in *Btg1*-null mice the EGL at P14 presented a great increase of thickness with respect to the normal condition, becoming hyperplastic (74% increase; Fig. 1A,C; *Btg1*<sup>-/-</sup> vs *Btg1*<sup>+/+</sup>,  $p < 0.00001$ ). This is a striking feature, given that normally from P7 to P14 the EGL thickness gradually decreases, as the GCPs migrate to the internal layers. As a whole, this indicates that the absence of *Btg1* increases not only the number of proliferating GCPs but also prolongs their period of proliferative expansion.

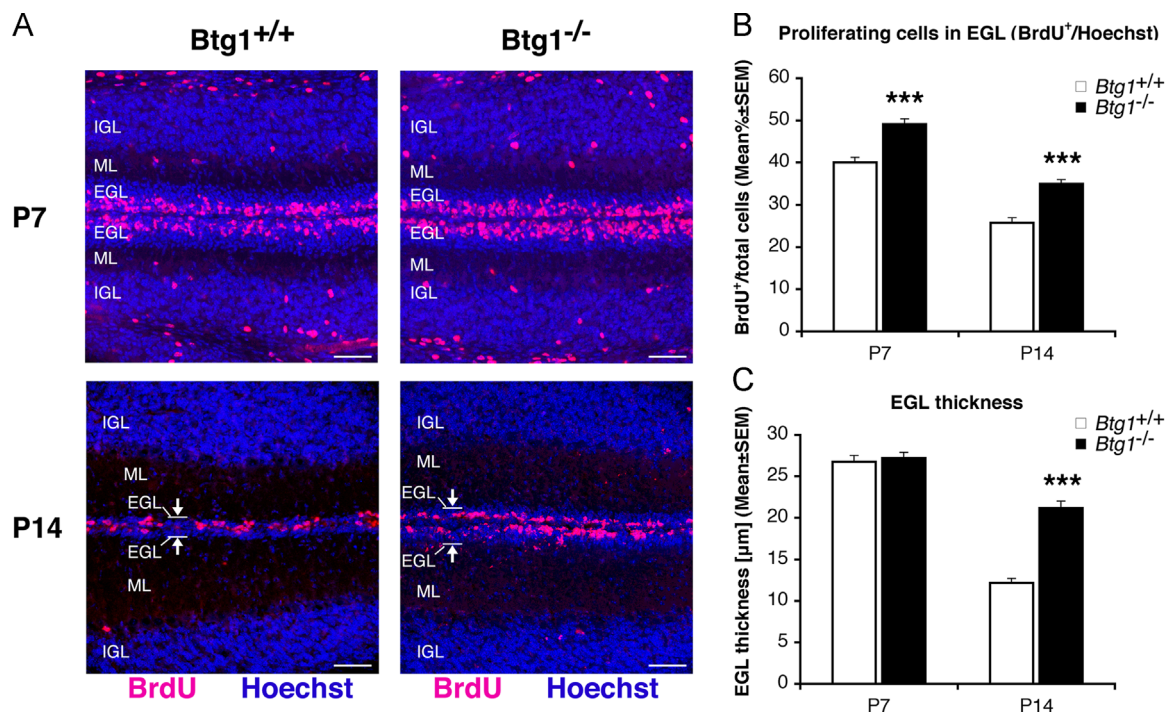


**Fig. 1.** Ablation of *Btg1* causes a strong increase of proliferating GCPs in the EGL, accompanied by an increase of the EGL thickness at P14. (A) Representative confocal images of GCPs that have entered the cell cycle S-phase, within the EGL of P7 or P14 mice either *Btg1*-null or wild-type, identified as BrdU<sup>+</sup> cells after a short pulse of BrdU (1 h). Sections are counterstained with Hoechst 33258 to visualize the EGL and the granule neurons and precursors contained. The greater width of two opposed neighboring EGLs of *Btg1*-null mice at P14 is indicated by two opposed arrows. Scale bar, 50 μm. (B) Analysis in the EGL of P7 or P14 *Btg1*<sup>-/-</sup> and *Btg1*<sup>+/+</sup> mice of the number of GCPs that have entered the S-phase of cell cycle, measured as mean ± SEM percentage ratio between number of BrdU<sup>+</sup> cells and total number of cells (visualized by Hoechst 33258; BrdU labeling index). Three mice for each genotype were analyzed. (C) Width of the EGL, calculated by measuring the average distance ± SEM between the pial surface and the border of the ML, in the same sections analyzed in (B). Three mice for each genotype were analyzed. (B,C) \*\*\*  $p < 0.001$  vs wild-type, Student's *t* test.

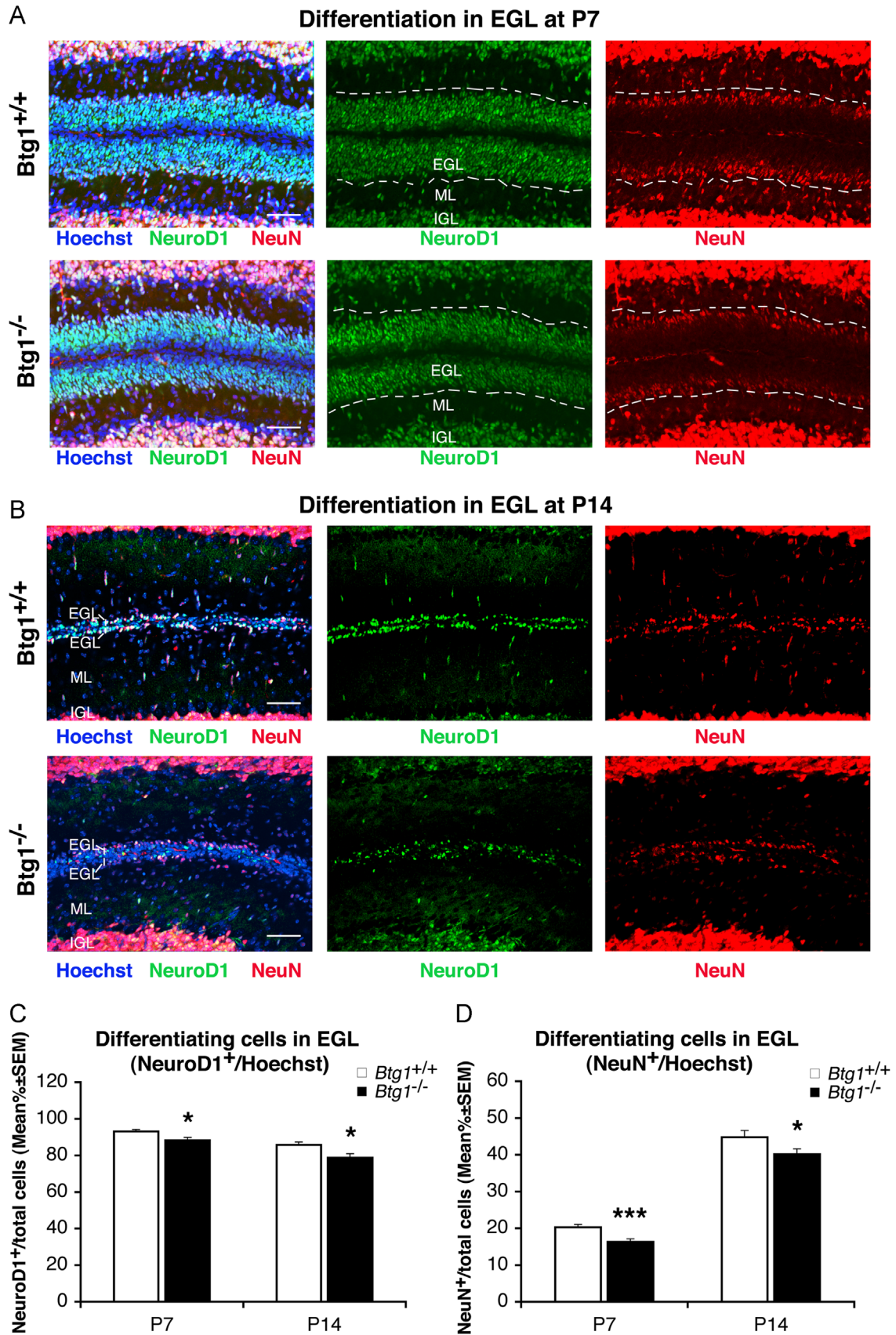


**Fig. 2.** Ablation of *Btg1* reduces the differentiation of GCPs in the EGL. (A,B) Representative confocal images of GCPs in the EGL of *Btg1*-null and wild-type mice, labeled with the early and the late differentiation markers NeuroD1 and NeuN, respectively, in P7 (A) and P14 mice (B). Sections are counterstained with Hoechst 33258 to visualize the EGL and the ML and IGL. In (A) the EGL boundaries are indicated by a white broken line. Scale bar, 50  $\mu$ m. (C,D) Quantitative analysis of GCPs expressing NeuroD1 (C) or NeuN (D) in the EGL of P7 and P14 *Btg1*<sup>-/-</sup> and *Btg1*<sup>+/+</sup> mice. Data are mean  $\pm$  SEM percentage ratio between the number of NeuroD1<sup>+</sup> or NeuN<sup>+</sup> GCPs and the total number of GCPs within the EGL, labeled by Hoechst 33258. Three mice for each genotype were analyzed. \*  $p < 0.05$  or \*\*\*  $p < 0.001$  vs wild-type, Student's *t* test.

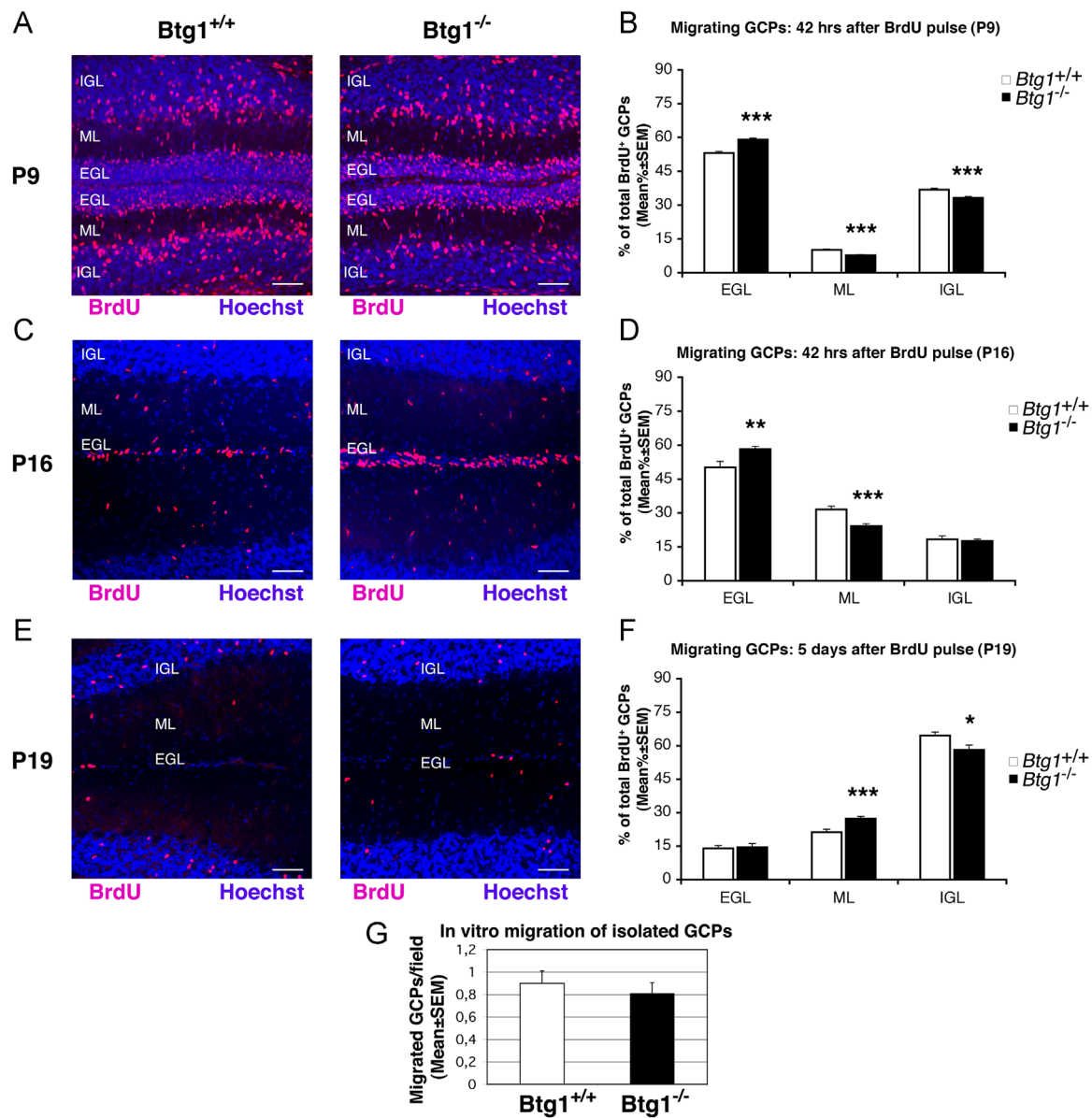


**Fig. 3.** Ablation of Btg1 reduces the migration of GCPs from EGL to molecular and internal granular layers. (A,C,E) Representative confocal images of GCPs migrating from the EGL, identified as BrdU<sup>+</sup> cells in Btg1-null and wild-type mice; P7 mice or P14 mice were injected with BrdU and analyzed after 42 h (A,C, respectively) or after 5 days (E). Sections are counterstained with Hoechst 33258 to visualize the EGL and the IGL. Scale bars, 50  $\mu$ m. (B,D,F) Quantification of GCPs migrating from the EGL either 42 h after BrdU injection in P7 mice (B), or 42 h after BrdU injection in P14 mice (D), or 5 days after BrdU injection in P14 mice (F), represented as mean  $\pm$  SEM percentage ratio of BrdU<sup>+</sup> cells in either the EGL, ML, or IGL, to the total BrdU<sup>+</sup> cells. Three mice per genotype were analyzed. \*  $p < 0.05$ , \*\*  $p < 0.01$  or \*\*\*  $p < 0.001$  vs wild-type, Student's *t* test. (G) Test of the intrinsic ability to migrate of purified Btg1-null GCPs, by a modified Boyden chamber. GFP-positive GCPs were isolated by FACS from P7 cerebellum of GFP/Btg1<sup>-/-</sup> and GFP/Btg1<sup>+/+</sup> mice, and were directly seeded in the upper chamber. The GFP-positive GCPs migrated to the lower side of the membrane were counted after 16 h. Mean cell number per field  $\pm$  SEM were obtained from two separate experiments, counting about 40 fields per well (at least 2 wells per experiment). The number of migrated Btg1-null GCPs did not significantly change, relative to Btg1 wild-type GCPs.

As a next step, we analyzed the differentiation of GCPs in the EGL. For this, GCPs were labeled at P7 and P14 with the neural markers NeuroD1 and NeuN. NeuroD1 labels in the EGL the recently differentiated GCPs and is necessary for their differentiation (Miyata et al., 1999), whereas NeuN marks differentiated granule neurons, detectable at the inner border of the EGL (Weyer and Schilling, 2003). At P7 and P14 the percentage of NeuroD1-positive GCPs as well as of NeuN-positive granule neurons was reduced slightly although significantly, relative to control mice (Fig. 2A–D; NeuroD1: at P7 and at P14, Btg1<sup>-/-</sup> vs Btg1<sup>+/+</sup>  $p = 0.01$ ; NeuN: Btg1<sup>-/-</sup> vs Btg1<sup>+/+</sup>, at P7  $p = 0.0007$ , and at P14  $p = 0.04$ ).

Subsequently, we measured the migration of GCPs from the EGL. First, the GCPs were labeled at P7 with an injection of BrdU,

and after 42 h BrdU-labeled GCPs were counted in each layer—EGL, ML and IGL—as percent ratio to the total number of BrdU<sup>+</sup> cells present in all layers. As shown in Fig. 3, in cerebella of Btg1-null mice the percentage of BrdU-labeled GCPs migrated in the ML and in the IGL after 42 h resulted significantly reduced, relative to control cerebella (Fig. 3A,B; Btg1<sup>-/-</sup> vs Btg1<sup>+/+</sup>, 24% and 10% decrease in ML and IGL, respectively;  $p < 0.00001$  in ML and  $p = 0.0002$  in IGL). In parallel, the number of Btg1-null BrdU<sup>+</sup> GCPs in the EGL was higher, as a greater number of them tended to remain locally (Fig. 3A,B;  $p < 0.00001$ ).

Similarly, when the GCPs migrating out of the EGL were analyzed at P16, 42 h after a BrdU injection, in cerebella of Btg1-null mice the percentage of BrdU-labeled GCPs migrated to the ML was

significantly reduced, whereas no difference was observed in the IGL, relative to control cerebella (Fig. 3C,D;  $Btg1^{-/-}$  vs  $Btg1^{+/+}$ , 23% decrease in ML,  $p=0.00008$ ); correspondingly, the number of  $BrdU^{+}$  GCPs was higher in the  $Btg1$ -null EGL (Fig. 3C,D;  $p=0.006$ ).

Finally, given the hyperplastic EGL observed in  $Btg1$ -null mice, we checked whether the migration from the EGL was still continuing at a later period, i.e., at P19, 5 days after a  $BrdU$  injection. In  $Btg1$ -null mice we observed a paradoxical increase of GCPs migrated to the ML, accompanied by a decrease within the IGL, relative to control mice (Fig. 3E,F;  $Btg1^{-/-}$  vs  $Btg1^{+/+}$ , 28% increase in ML,  $p=0.0004$ ; 10% decrease in IGL,  $p=0.01$ ). This clearly indicated that the migration of GCPs along the route from ML to IGL was delayed, plausibly with a prolongation of the whole process of migration from the EGL to IGL.

These data suggest that the ablation of  $Btg1$  affects not only the proliferation of GCPs, but also their differentiation and migration outside the EGL until P14–19, i.e., throughout the whole period of GCPs amplification.

However, given the critical effect that the increase of proliferation and delayed exit from the cell cycle of GCPs can have on differentiation and migration, we sought to ascertain whether the reduced migration of  $Btg1$ -null GCPs was cell autonomous. First we generated  $GFP/Btg1^{-/-}$  mice, by crossing the  $Btg1^{-/-}$  mice to  $Math1$ -green fluorescent protein mice ( $Math1$ -GFP), where the  $Math1$  enhancer drives the expression of GFP in proliferating GCPs (Lumpkin et al., 2003). Then, we analyzed the ability of purified GCPs, isolated at P7 from  $GFP/Btg1^{-/-}$  mice as  $GFP^{+}$  cells by FACS, to migrate in a modified Boyden chamber, as previously described (Lu et al., 2001). In brief, a membrane filter with uniform pore size divides upper and lower chambers. GCPs are seeded in the upper chamber, and the number of those that have migrated to the lower surface of the filter is determined. The number of  $GFP/Btg1^{-/-}$  GCPs that migrated to the lower chamber did not differ from

$GFP/Btg1^{+/+}$  GCPs (Fig. 3G;  $p=0.61$ ). This conclusively indicates that the ablation of  $Btg1$  does not affect the intrinsic ability of GCPs to migrate. In contrast, we observed previously that GCPs lacking the family-related gene  $Tis21$  show a marked decrease of migration in the same assay (Farioli-Vecchioli et al., 2012a).

We also evaluated the survival of GCPs in the EGL at P7 and P14. We found that the percentage of GCPs undergoing apoptosis increased significantly at P7, while no difference relative to wild-type was observed at P14, as detected by positivity to cleaved Caspase-3 (Fig. 4A,B; at P7,  $Btg1^{-/-}$  vs  $Btg1^{+/+}$ ,  $p=0.0002$ ). In fact, at P14 in  $Btg1^{-/-}$  EGL the absolute number of apoptotic cells increased proportionally to the increased total number of GCPs present in the thicker EGL (Fig. 4A,C; at P14,  $Btg1^{-/-}$  vs  $Btg1^{+/+}$ ,  $p<0.00001$ ). Thus, in  $Btg1$ -null GCPs a net increase of apoptosis occurred when the ratio of proliferating GCPs is at the peak, i.e. at P7, rather than during the prolonged increase of proliferation evident at P14.

We further sought to assess whether the defective cerebellar development evident in  $Btg1$ -null mice could imply the family-related gene  $Tis21$  as a molecular partner of  $Btg1$  action. Thus, we measured two key parameters of the GCPs, i.e., their proliferation and migration, in  $Btg1^{-/-}$ ,  $Tis21^{-/-}$ , or in double knockout ( $Btg1^{-/-}/Tis21^{-/-}$ ) and in control  $Btg1^{+/+}/Tis21^{+/+}$  (referred to as wild-type) mice at P7. The percentage of proliferating GCPs in the EGL at P7, identified by incorporation of  $BrdU$  after 1 h pulse, did not change in  $Tis21$  knockout mice, while it increased to the same extent in  $Btg1$  knockout and in double knockout mice, relative to wild-type mice (Fig. 5A,B;  $Btg1^{-/-}$  or  $Btg1^{-/-}/Tis21^{-/-}$  vs wild-type,  $p<0.00001$  with 21% and 18% increase, respectively). This indicates that the proliferative control of the GCPs depends essentially on  $Btg1$ .

The migration of the GCPs outside the EGL was analyzed as above, by measuring the percent ratio of  $BrdU^{+}$  GCPs in each layer

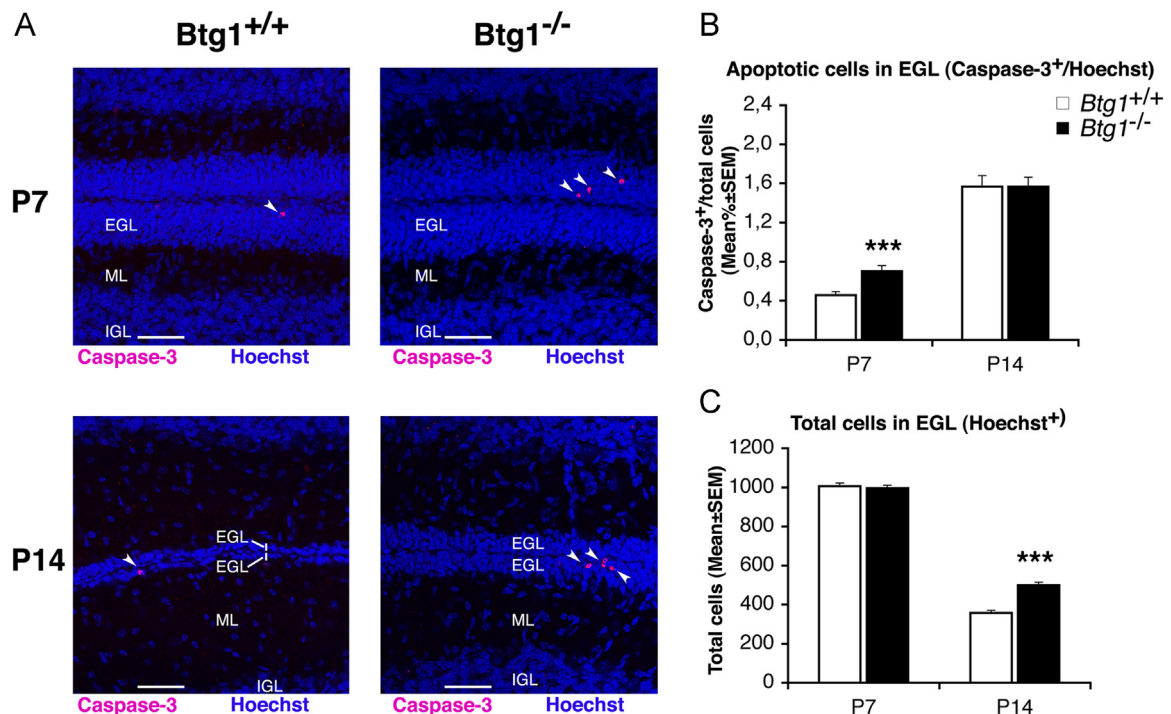


**Fig. 4.** Ablation of  $Btg1$  increases the apoptosis of GCPs in the EGL. (A) Representative confocal images of apoptotic GCPs, identified as cleaved Caspase-3<sup>+</sup> cells (white arrowheads), in the EGL of P7 or P14  $Btg1$ -null and wild-type mice. Scale bar, 50  $\mu$ m. (B) Apoptotic GCPs in the EGL of P7 and P14  $Btg1^{-/-}$  and  $Btg1^{+/+}$  mice, quantified as mean  $\pm$  SEM percentage ratio between the number of cleaved Caspase-3<sup>+</sup> GCPs and the total number of GCPs within the EGL, labeled by Hoechst 33258. (C) The total number of GCPs (Hoechst<sup>+</sup>) was greater in the  $Btg1^{-/-}$  EGL at P14, indicating that the absolute number of cleaved Caspase-3<sup>+</sup> GCPs was also greater. (B,C) Three mice for each genotype were analyzed; \*\*\*  $p<0.001$  vs wild-type, Student's  $t$  test.

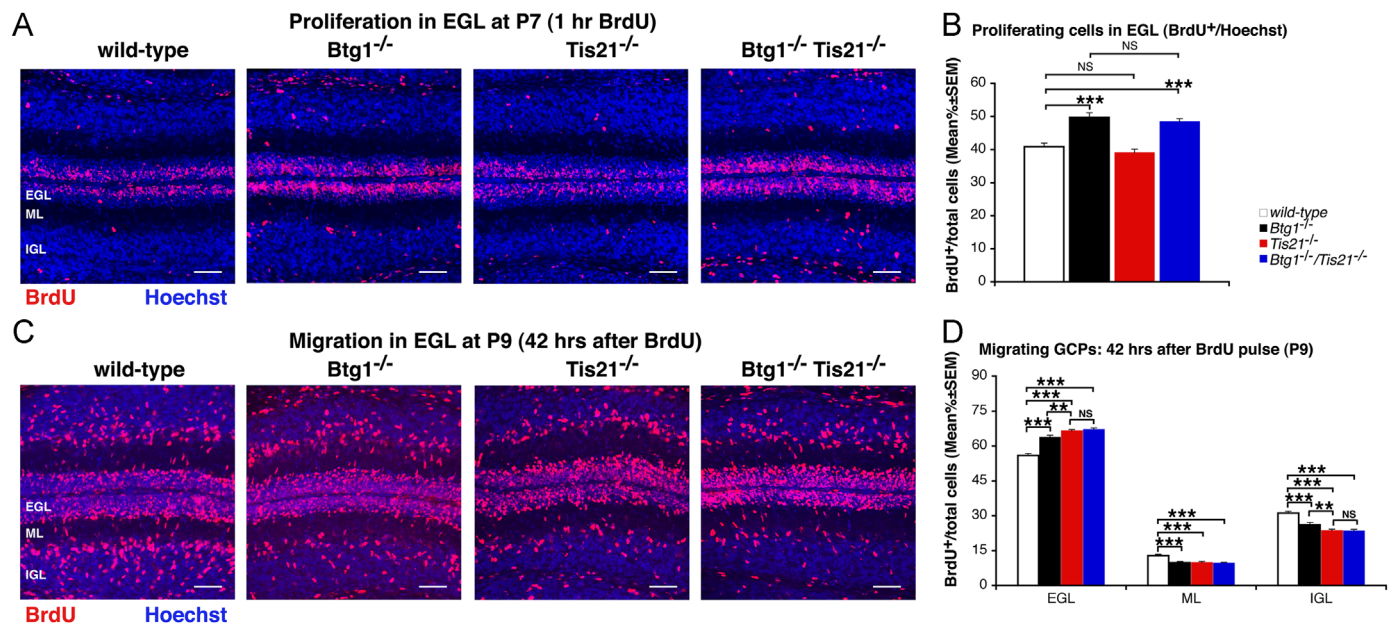


**Fig. 5.** Double Btg1/Tis21 knockout mice show that Btg1 and Tis21 primarily control proliferation and migration of the GCPs, respectively. (A) Representative confocal images of proliferating GCPs in the EGL of wild-type, Btg1-null, Tis21-null or double knockout P7 mice, identified as BrdU<sup>+</sup> cells after a 1 h pulse of BrdU. Sections are counterstained with Hoechst 33258 to visualize the whole of EGL granule neurons and precursors. Scale bar, 50  $\mu$ m. (B) Analysis in the EGL of P7 wild-type, Btg1<sup>-/-</sup>, Tis21<sup>-/-</sup> or double knockout mice of the GCPs that have entered the S-phase of the cell cycle (measured as mean  $\pm$  SEM percentage ratio between number of BrdU<sup>+</sup> cells in EGL and total number of cells, visualized by Hoechst 33258). Three mice for each genotype were analyzed. \*\*\*  $p < 0.001$  vs wild-type, Student's *t* test. (C) Representative confocal images of GCPs migrating outside the EGL, identified as BrdU<sup>+</sup> cells in the four genotypes; P7 mice were injected with BrdU and analyzed after 42 h. Sections are counterstained with Hoechst 33258 to visualize the ML and the IGL. Scale bars, 50  $\mu$ m. (D) Quantification of GCPs migrating from the EGL 42 h after BrdU injection in P7 mice, represented as mean  $\pm$  SEM percentage ratio of BrdU<sup>+</sup> cells in either the EGL, ML, or IGL to the total BrdU<sup>+</sup> cells. Three mice per genotype were analyzed. \*\*  $p < 0.01$  or \*\*\*  $p < 0.001$ , Student's *t* test.

to the total number of BrdU<sup>+</sup> cells in all three layers (EGL, ML and IGL), 42 h after a BrdU pulse in P7 mice. In the EGL the percent ratio of non migrating BrdU<sup>+</sup> GCPs increased significantly in all mutants relative to the control, but the BrdU<sup>+</sup> GCPs in both Tis21-null and double mutant mice were significantly higher than in Btg1-null mice (Fig. 5C,D; EGL: Btg1<sup>-/-</sup> or Tis21<sup>-/-</sup> or Btg1<sup>-/-</sup>/Tis21<sup>-/-</sup> vs wild-type,  $p < 0.0001$ ; Tis21<sup>-/-</sup> or Btg1<sup>-/-</sup>/Tis21<sup>-/-</sup> vs Btg1<sup>-/-</sup>,  $p = 0.006$  for both). Consistently, in ML and IGL the GCPs migrated were significantly less. In particular, in the IGL the percent ratio of BrdU<sup>+</sup> GCPs migrated was significantly lower than control in all mutant mice, but, notably, BrdU<sup>+</sup> GCPs in Tis21-null and in double mutant mice were both significantly lower than in Btg1-null mice (Fig. 5C,D; IGL: Btg1<sup>-/-</sup> or Tis21<sup>-/-</sup> or Btg1<sup>-/-</sup>/Tis21<sup>-/-</sup> vs wild-type,  $p < 0.00001$ ; Tis21<sup>-/-</sup> or Btg1<sup>-/-</sup>/Tis21<sup>-/-</sup> vs Btg1<sup>-/-</sup>,  $p = 0.008$  and  $p = 0.009$ , respectively). As a whole, this indicated that Tis21 controls the migration of GCPs, while the less evident decrease of migration observed in Btg1-null mice, given that Btg1 does not affect the intrinsic ability of GCPs to migrate (Fig. 3G), may be consequence of the increased proliferation.

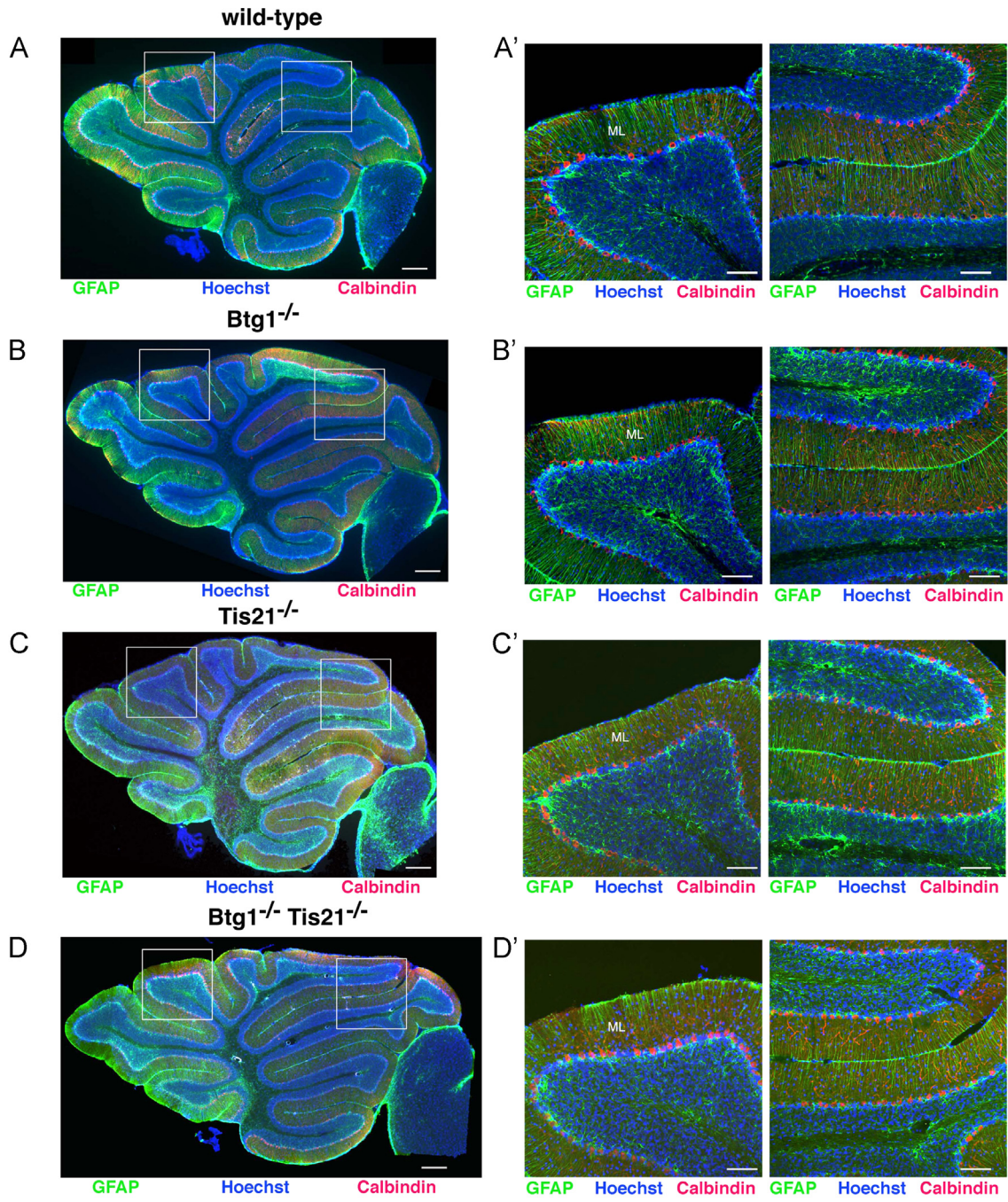
Next, we tested whether the altered developmental features of Btg1-null cerebella, i.e., the hyperplastic EGL consequent to increased proliferation and impaired differentiation and migration of GCPs, resulted in changes of the gross cerebellar morphology after completion of the cerebellar development, at P60. In Btg1-null adult mice light but significant differences occurred in the cerebellar cortex length, which is indicative of the complexity of foliation and length of lobules and depends on proliferation and migration of GCPs (Sudarov and Joyner, 2007) and in the IGL area as well as in the cerebellar volume (Fig. 6A,A',B,B',E; Btg1<sup>-/-</sup> vs wild-type: cortex length  $p = 0.003$ , IGL area  $p = 0.0001$ , cerebellar volume  $p = 0.01$ ). However, the Bergmann's glia, which plays a key role during embryogenesis in directing the radial migration of

Purkinje cells from the ventricular zone to the outer cerebellum and after birth the migration of GCPs from the EGL to the inner layers (Wang and Wechsler-Reya 2014; Hatten 1999), appeared normal (Fig. 6B,B'). Also the number of Purkinje cells did not change in Btg1-null mice (Fig. 6B,B'), thus ruling out external variables in the altered migration of Btg1-null GCPs. No evident change in cerebellar morphology was observed in mice with deletion of the family-related gene Tis21 (Fig. 6C,C',E). Notably, however, double Btg1/Tis21 knockout mice presented evident changes of the gross cerebellar morphology in adult mice (at P60), with significant increases in cerebellar volume, ML and IGL area and cortex length, relative to wild-type or to Btg1 and Tis21 knockouts (Fig. 6D,D',E; Btg1<sup>-/-</sup>/Tis21<sup>-/-</sup> vs wild-type: cortex length, ML and IGL area  $p < 0.0001$ , cerebellar volume  $p = 0.007$ ; Btg1<sup>-/-</sup>/Tis21<sup>-/-</sup> vs Btg1<sup>-/-</sup>: cortex length, ML and IGL area  $p \leq 0.02$ ; Btg1<sup>-/-</sup>/Tis21<sup>-/-</sup> vs Tis21<sup>-/-</sup>: cortex length, ML and IGL area  $p \leq 0.002$ , cerebellar volume  $p = 0.02$ ). Thus, while the postnatal alterations of migration of Tis21-null GCPs appear to be compensated during the late developmental stages, the altered development of Btg1-null and double mutant GCPs results in permanent morphological defects.

### 3.2. Defective motor coordination in adult Btg1<sup>-/-</sup>, Tis21<sup>-/-</sup> and Btg1<sup>-/-</sup>/Tis21<sup>-/-</sup> mice

Alteration of the postnatal cerebellar development can be associated with permanent defects of motor functions. To test this possibility, we analyzed wild-type and mutant mice (Btg1<sup>-/-</sup>, Tis21<sup>-/-</sup> and Btg1<sup>-/-</sup>/Tis21<sup>-/-</sup>) in behavioral tests performed to evaluate their neuromotor functions.

First, we performed the rotarod test, which allows assessment of the fore- and hind limb motor coordination and balance in mice. This task is a measure of the cerebellar function, and mice with



**E**

Genotype	Cerebellar cortex length [mm]	ML area [mm <sup>2</sup> ]	IGL area [mm <sup>2</sup> ]	Cerebellar volume [mm <sup>3</sup> ]	Purkinje cells number (per field)
wild-type	19.65 ± 0.57	2.95 ± 0.08	2.41 ± 0.05	24.92 ± 0.30	26.68 ± 0.87
<i>Btg1</i> <sup>-/-</sup>	21.47 ± 0.57 * †	3.18 ± 0.07 †	2.75 ± 0.06 *** †	27.82 ± 0.61 *	27.24 ± 0.54
<i>Tis21</i> <sup>-/-</sup>	20.44 ± 0.50 †††	3.14 ± 0.07 ††	2.50 ± 0.05 †††	25.78 ± 0.92 †	26.67 ± 0.59
<i>Btg1</i> <sup>-/-</sup> <i>Tis21</i> <sup>-/-</sup>	23.25 ± 0.46 ***	3.46 ± 0.07 ***	3.01 ± 0.07 ***	29.84 ± 0.95 **	28.11 ± 0.59

**Fig. 6.** Adult cerebella of *Btg1*<sup>-/-</sup> and *Btg1*<sup>-/-</sup>/*Tis21*<sup>-/-</sup> mice display altered morphology. (A,A',B,B') Representative confocal images of P60 *Btg1*<sup>-/-</sup> mice show slight but significant differences relative to wild-type mice in cerebellar volume, while the Bergmann's glia (labeled in green by GFAP) or the presence of Purkinje cells (at the border of the molecular layer [ML], labeled in red by Calbindin), do not differ. (A',B') White boxes: area at higher magnification, shown in lower panels. (C,C') *Tis21*<sup>-/-</sup> cerebella do not differ morphologically from wild-type, whereas (D,D') *Btg1*<sup>-/-</sup>/*Tis21*<sup>-/-</sup> adult cerebella show a larger size than wild-type cerebella. (A,A'-D,D') Scale bars: 300 μm; enlargement, 100 μm. (E) Quantified features of the cerebellar morphology for each genotype at P60. Cerebellar cortex length, ML and IGL area were calculated for the whole cerebellum. Mean ± SEM from at least three mice for each genotype. \* *p* < 0.05, \*\* *p* < 0.01 and \*\*\* *p* < 0.001 vs wild-type; † *p* < 0.05, †† *p* < 0.01 and ††† *p* < 0.001 vs double knockout (Student's *t* test).

severe motor coordination problems have difficulties remaining on the rotating rod (Crawley, 1999). The test, performed for four days, was carried out on both male and female mice, as preliminary tests performed on wild-type mice did not show significant differences between sexes (data not shown). From the beginning both single and double mutant mice showed a great, significant reduction of the time to fall off the accelerated rotarod compared with wild-type mice, thus showing deficits in motor coordination and balance (Fig. 7A,C;  $Btg1^{-/-}$  or  $Tis21^{-/-}$  or  $Btg1^{-/-}/Tis21^{-/-}$  vs wild-type,  $p < 0.03$  or lower, in all tests). Notably, double mutant mice showed the shortest latencies to fall. A significant impairment was observed for each mutant genotype, relative to the wild-type, also when male and female results were analyzed separately (data not shown), confirming that our results obtained in the rotarod test were not sex-dependent. To further check whether the performance of mice in the rotarod test was affected by alteration of the neuromuscular strength, we performed the horizontal bar test, which reveals any possible deficit in muscle functions. No significant difference in time to fall from the horizontal bar was observed (also in male and female mice analyzed separately), thus ruling out a deficit in neuromuscular strength (Fig. 7B,C;  $Btg1^{-/-}$  or  $Tis21^{-/-}$  or  $Btg1^{-/-}/Tis21^{-/-}$  vs wild-type,  $p \geq 0.57$ ). In addition, the body weight of the mice resulted equivalent amongst the different genotypes (Fig. 7D; shown separately for male and female mice). Hence, the developmental defects caused by ablation of  $Btg1$  or  $Tis21$  resulted in permanent functional cerebellar deficits.

### 3.3. Control of cyclin D1 by $Btg1$

$Btg1$  has been shown to inhibit the cell cycle (Rouault et al., 1992); in fact, its overexpression in breast cancer cells and in granulosa cells of the ovary causes arrest in the G0-G1 phase (Zhu et al. 2013; Li et al., 2009). We have recently observed, moreover, that in neural stem cells of the dentate gyrus  $Btg1$  acts by controlling the length of the S-phase (Farioli-Vecchioli et al., 2014b). Thus, we sought to define at which stage of the cell cycle  $Btg1$  is required in the cerebellum. To this end, we analyzed whether the D cyclins, controlling the G1-S phase, and A cyclin, which is maximally expressed at the G2 phase and controls the switch from prometaphase to metaphase (Baumann, 2013), were involved in the proliferation of GCPs. We observed a small but highly significant increase of GCPs expressing cyclin D1 (cyclin D1<sup>+</sup>) in the EGL of  $Btg1$ -null mice at P7, relative to  $Btg1$  wild-type (Fig. 8A,B; 11% increase of cyclin D1<sup>+</sup> GCPs on the total number of GCPs;  $p=0.004$ ). In parallel, no significant change was observed in cyclin D2<sup>+</sup> or cyclin A<sup>+</sup> GCPs (Fig. 8B,  $Btg1^{-/-}$  vs  $Btg1^{+/+}$ ,  $p=0.82$  for cyclin D2<sup>+</sup> and  $p=0.94$  for cyclin A<sup>+</sup> GCPs).

Thus, we sought to further investigate the implication of cyclins in the mechanism of  $Btg1$ , and in particular the specificity of cyclin D1 involvement. We therefore conducted further analyses in a cell line of immortalized GCPs (C17.2 cell line; Ryder et al., 1990).

In the first place we checked, by either silencing or over-expressing  $Btg1$ , whether the regulation of proliferation by  $Btg1$  in the GCP cell line was similar to that in GCPs in vivo. We identified

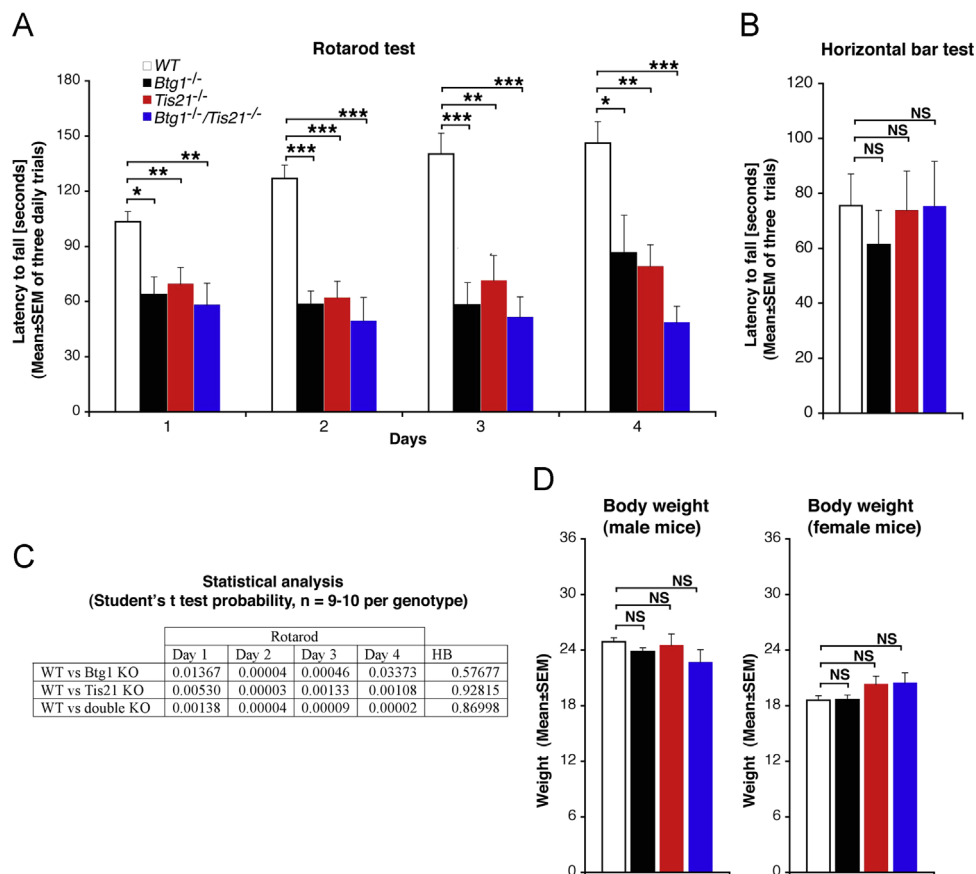


**Fig. 7.** Impaired motor coordination in adult  $Btg1^{-/-}$ ,  $Tis21^{-/-}$  and  $Btg1^{-/-}/Tis21^{-/-}$  mice. (A) Rotarod and (B) bar holding performances in P60 mice of the indicated genotype. (A) Quantification for each genotype of the latency to fall off the rotating rod over 4 daily tests (each column is the average ± SEM of three trials per day); the latency of mutant mice is significantly reduced at all time-points, relative to wild-type. (B) Quantification of the latency to fall from a thin metallic bar (average ± SEM of three trials). (C) Summary of the statistical analysis. (D) Quantification of the body weight for each genotype, shown separately for male and female mice. (A,B,D) wild-type (white),  $Btg1^{-/-}$  (black),  $Tis21^{-/-}$  (red) and  $Btg1^{-/-}/Tis21^{-/-}$  (blue). \*  $p < 0.05$ , \*\*  $p < 0.01$ , \*\*\*  $p < 0.001$ , Student's  $t$ -test, comparison of mutant vs wild-type mice.  $n=9-10$  mice for each genotype.

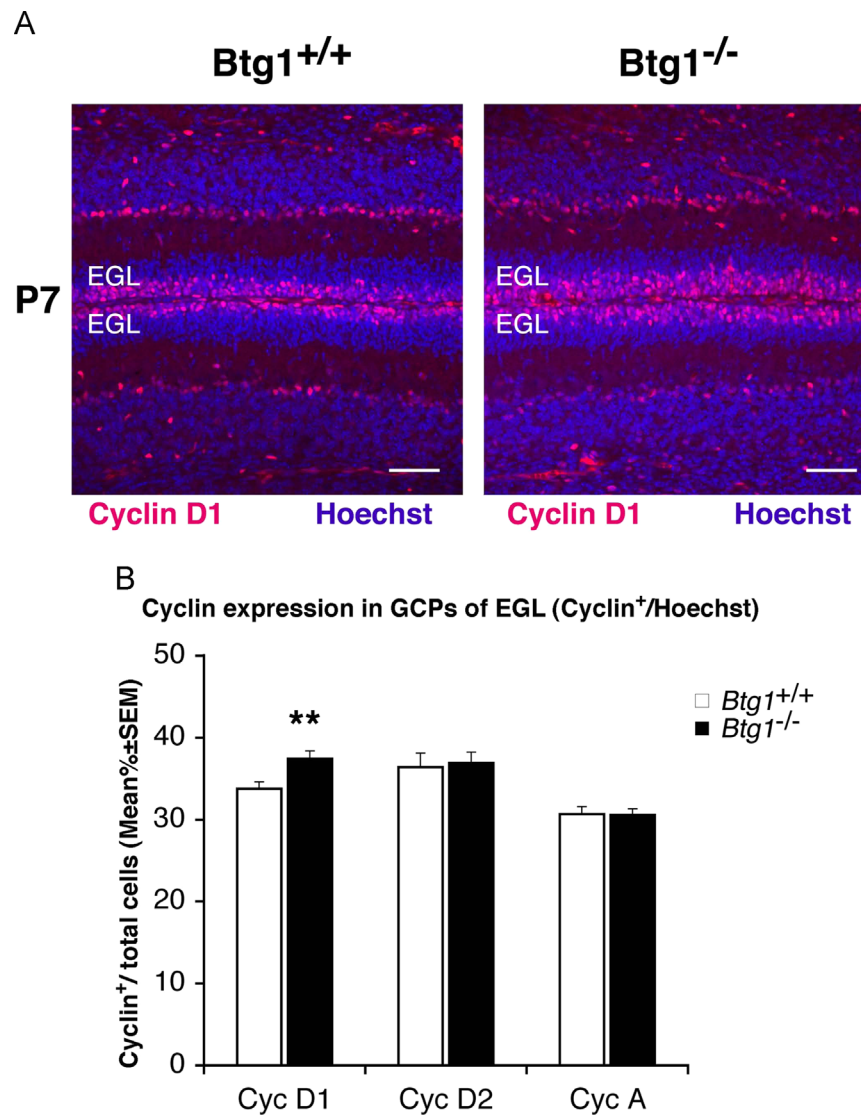


**Fig. 8.** Ablation of Btg1 increases the number of cyclin D1-positive GCPs. (A) Representative confocal images of GCPs expressing cyclin D1 within the EGL of P7 mice, either Btg1-null or wild-type. Sections are counterstained with Hoechst 33258 to visualize the granule neurons and precursors in the EGL. Cyclin D1<sup>+</sup> cells are more frequent in the Btg1-null EGL. Scale bar, 50  $\mu$ m. (B) Quantification in the EGL of P7 Btg1<sup>-/-</sup> and Btg1<sup>+/+</sup> mice of the number of GCPs expressing cyclin D1, cyclin D2 or cyclin A, measured as mean  $\pm$  SEM percentage ratio between number of cyclin D1<sup>+</sup>, cyclin D2<sup>+</sup> or cyclin A<sup>+</sup> cells and the total number of cells (visualized by Hoechst 33258). Three mice for each genotype were analyzed. \*\*  $p < 0.01$  vs wild-type, Student's *t* test.

an shRNA specifically targeting Btg1 (shBtg1) and cloned it in the retroviral vector pSUPER.retro-neo-GFP, obtaining pSUPER.retro-neo-GFP-shBtg1 to generate the corresponding retrovirus; pSUPER.retro-neo-GFP-shLUC was generated to obtain control shRNA retroviruses targeting the luciferase mRNA sequence (shLUC). Indeed, the silencing of Btg1 by the shBtg1-expressing retrovirus in the C17.2 line of immortalized GCPs reduced of 81% the Btg1 mRNA expression relative to control shLUC-expressing retrovirus (Fig. 9A, shBtg1 vs shLUC,  $p < 0.006$ ), and caused increases of BrdU incorporation (Fig. 9B,  $p = 0.02$ ) and, especially, of cyclin D1 protein levels (Fig. 9C); in contrast cyclin A did not increase and cyclins D2 and B1 showed a small increase (Fig. 9C, 203% increase of cyclin D1, 12% increase of cyclin D2, 25% decrease of cyclin A, and 26% increase of cyclin B1, as by densitometry analysis after normalization to  $\alpha$ -tubulin).

In parallel we analyzed also the effect of overexpressing Btg1 in immortalized GCPs by transfecting the expression vector pSCT-HA-FLAG-Btg1 or pSCT- $\beta$ Gal as control. We found that overexpression of Btg1 in C17.2 immortalized GCPs caused a significant

inhibition of the transition from the G1 to S phase of the cell cycle, as judged by BrdU incorporation (measuring the percent ratio of BrdU<sup>+</sup>Btg1-Flag<sup>+</sup> or BrdU<sup>+</sup> $\beta$ Gal<sup>+</sup> cells to the total number of Btg1-Flag<sup>+</sup> or  $\beta$ Gal<sup>+</sup> cells, respectively; Fig. 9D,  $p < 0.0001$ ). Moreover, overexpression of Btg1 in C17.2 cells caused a quite selective, though not exclusive, inhibition of cyclin D1 protein (50% decrease, as judged by densitometry scanning; moreover, cyclin D2 and cyclin B1 decreased of about 8% while cyclin A and cyclin E increased slightly; Fig. 9E,F).

In conclusion, these data suggest that the regulation of proliferation by Btg1 in immortalized GCPs is comparable to that observed in GCPs in vivo, with a main role played by cyclin D1.

Thus, we performed a functional analysis in GCP (C17.2 cells) to ascertain the specificity of the control of cyclin D1 by Btg1, by analyzing the ability of the different cyclins to reverse the f0050\_6887Btg1-dependent inhibition in the S phase entry. C17.2 cells were transiently transfected with Btg1 in either the presence or the absence of cyclins and their specific cyclin-dependent kinase (CDK) partner, and the entry of cells into S phase was checked

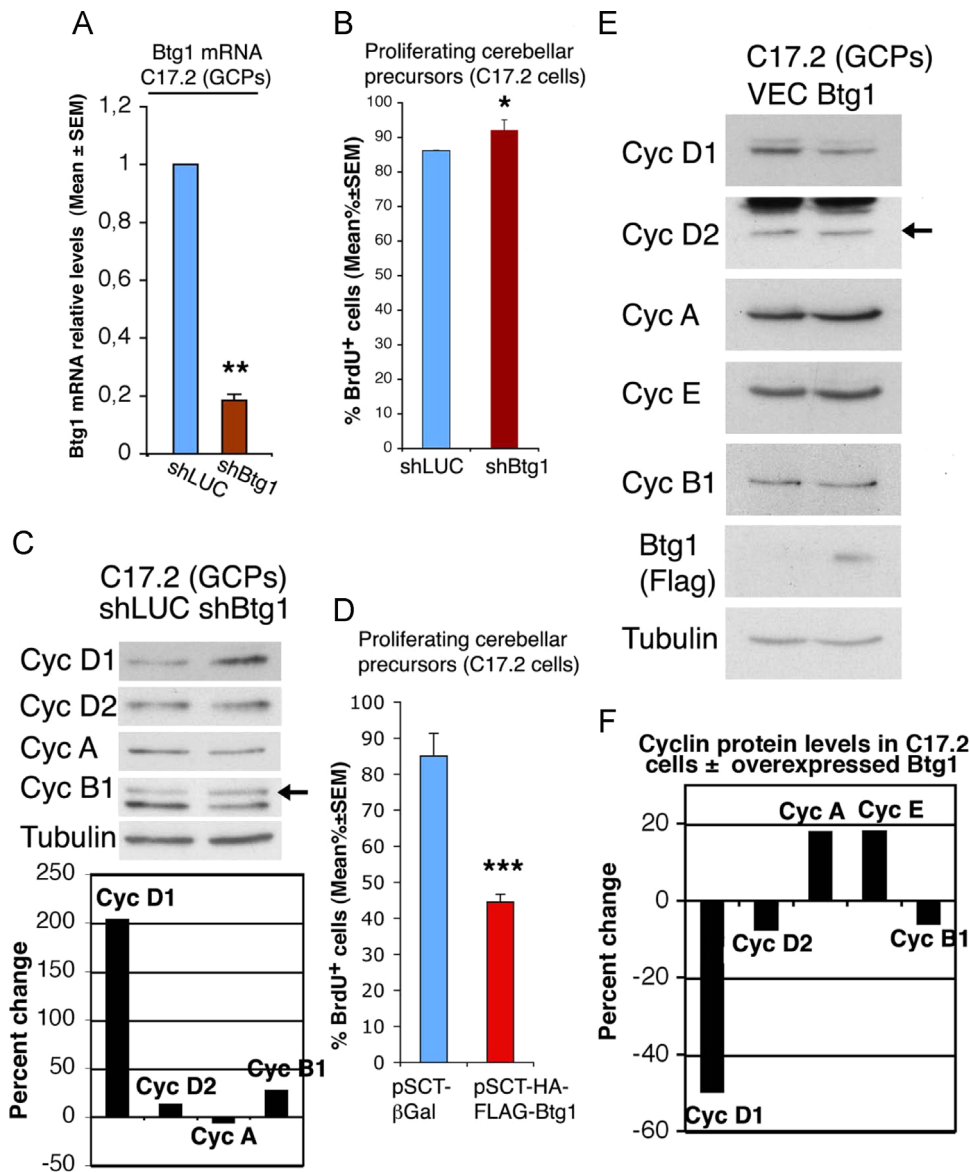


**Fig. 9.** Btg1 inhibits the proliferation of immortalized GCPs by regulating cyclin D1. (A–C), Increase of proliferation and of cyclin D1 levels after silencing Btg1. (A) Analysis of Btg1 mRNA expression in C17.2 immortalized GCPs, infected with retroviruses generated by the pSUPER.retro-neo-GFP vector expressing a Btg1-specific shRNA sequence (shBtg1) or expressing Luciferase-specific shRNA sequence (shLUC). 72 h after infection, cells were analyzed. TBP was used to normalize data. \*\*  $p < 0.01$  or \*\*\*  $p < 0.001$ , Student's *t* test. (B) Percentage of BrdU-incorporating C17.2 GCPs infected with the shBtg1- or shLUC-expressing retroviruses, after an 18 h BrdU pulse. Values are calculated as percent ratio of BrdU+GFP+ cells to the total number of GFP+ cells. For each group were counted more than 300 cells. Means  $\pm$  SEM values are from at least three independent experiments. \*  $p < 0.05$ , Student's *t* test. (C) Immunoblotting and densitometry analysis with anti-cyclins D1, D2, A or B1 antibodies in C17.2 GCPs after infection with the shBtg1- or shLUC-expressing retroviruses. (D–F) Inhibition of proliferation and of cyclin D1 expression by Btg1 overexpressed in C17.2 cells. C17.2 cells ( $1.5 \times 10^5$ ) were seeded onto 60-mm-diameter culture dishes. After 24 h, cells were transfected with either pSCT-HA-FLAG-Btg1 (5  $\mu$ g/dish), or with pSCT- $\beta$ Gal or pSCT empty plasmid (VEC; 5  $\mu$ g/dish), as indicated. Sixty hours after, transfected cells were subjected to either (D) analysis of proliferation, (E) protein extraction and immunoblotting with antibodies specific for the indicated cyclins. (D) BrdU-positive C17.2 cells overexpressing Btg1 were measured after an 18 h BrdU pulse as percentages of BrdU+ Btg1-Flag+ cells to the total number of Btg1-Flag+ cells; BrdU-positive cells expressing  $\beta$ Gal were calculated as percentages of BrdU+  $\beta$ Gal+ cells to the total number of  $\beta$ Gal+ cells. Mean  $\pm$  SEM values are from at least three independent experiments. \*\*\*  $p < 0.001$ , Student's *t* test. (E,F) Western blot in C17.2 cells and densitometry analysis; values are presented as percent change of protein expression in Btg1-transfected cells relative to VEC-transfected control cells, after normalization to the corresponding values of tubulin expression (the control base line is set to 0).

by means of BrdU incorporation (Fig. 10A,B). The ectopic expression of Btg1 inhibited about 50% the incorporation of BrdU (Fig. 10A,B; Btg1 vs  $\beta$ Gal control,  $p < 0.0001$ ). We observed that only cyclin D1 was able to induce full recovery of the DNA synthesis inhibited by Btg1 (94% recovery of the basal level, or 97% recovery when cyclin D1 was coexpressed with CDK4), while all the other cyclins (D2, D3, A, E, B1, B2), either with or without CDKs, counteracted only partially the inhibition of BrdU incorporation elicited by Btg1 (Fig. 10A,B; cyclin D1+ Btg1 vs  $\beta$ Gal

control,  $p = 0.08$ ; cyclin D1+CDK4+ Btg1 vs  $\beta$ Gal control,  $p = 0.32$ ; all other cyclins+ Btg1 vs  $\beta$ Gal,  $p < 0.01$  or lower).

Next, we sought to further test the selectivity of the role of cyclin D1 in the Btg1-dependent regulation of cell cycle. For this, we analyzed the ability of Btg1 to inhibit the S-phase progression in C17.2 cells where cyclin D1 expression was silenced by a retrovirus carrying an shRNA specifically targeting cyclin D1 (shcycD1). The shcycD1 sequence, identified by us, was cloned in the retroviral vector pSUPER.retro-puro-shcycD1 to generate the

corresponding retrovirus, and resulted effective in reducing cyclin D1 expression in C17.2 cells (Fig. 10C). Infected C17.2 cells (with shycyD1 or shLUC retroviruses) were transiently transfected with the pSCT-HA-FLAG-Btg1 or the control pSCT- $\beta$ Gal expression constructs, and BrdU incorporation was measured as the percentage ratio of double labeled cells, either BrdU<sup>+</sup>Btg1-Flag<sup>+</sup> or BrdU<sup>+</sup> $\beta$ Gal<sup>+</sup>, to the total number of Btg1-Flag<sup>+</sup> or  $\beta$ Gal<sup>+</sup> cells, respectively. Btg1 overexpression inhibited significantly BrdU incorporation in both control (shLUC) and cyclin D1-silenced (shycyD1) C17.2 cells (Fig. 10D,  $p=0.0001$  and  $p=0.001$ , respectively), but the inhibition was significantly lower in cyclin D1-silenced C17.2 cells, relative to shLUC control cells (Fig. 10D, shLUC<sup>+</sup>pSCT-HA-FLAG-Btg1 vs shycyD1<sup>+</sup>pSCT-HA-FLAG-Btg1,  $p=0.001$ ).

Additionally, given that the control of cyclins by Btg1 in fibroblasts resulted completely equivalent to that observed in C17.2 cells (data not shown), we also checked the ability of Btg1 to inhibit the S-phase progression in primary MEF cells explanted from a cyclin D1 knockout mouse, by measuring BrdU incorporation. In cyclin D1<sup>+/+</sup> and cyclin D1<sup>-/-</sup> MEF cells, transiently transfected with the pSCT-HA-FLAG-Btg1 or the control pSCT- $\beta$ Gal expression constructs, the expression of Btg1 (measured as above, as percentage ratio of double labeled BrdU<sup>+</sup>Btg1-Flag<sup>+</sup> or BrdU<sup>+</sup> $\beta$ Gal<sup>+</sup> cells), inhibited significantly BrdU incorporation only in cyclin D1<sup>+/+</sup> MEFs (58% decrease,  $p=0.01$ ); however, a slight non statistically significant decrease of BrdU incorporation was observed also in cyclin D1<sup>-/-</sup> MEFs ( $p=0.17$ ; Fig. 10E). As a whole, this confirms that Btg1 regulates S-phase progression mainly through cyclin D1.

#### 3.4. Btg1 inhibits proliferation of medulloblastoma cells

The results shown above indicated an inhibitory role of Btg1 in the proliferation of GCPs in vivo. Thus, we wished to evaluate whether Btg1 could inhibit the proliferation also in neoplastic cells from full-blown medulloblastoma. We therefore overexpressed Btg1 in the widely used medulloblastoma cell line DAOY, derived from the desmoplastic human subtype (Jacobsen et al., 1985). We observed that in this medulloblastoma cell line the overexpression of Btg1 was able to significantly inhibit proliferation of about 45%, as judged by incorporation of BrdU, with respect to control cultures infected with  $\beta$ Galactosidase-expressing vector (Fig. S1A,B).

## 4. Discussion

Our in vivo data show that Btg1 is required chiefly for the negative control of proliferation and, to a lesser extent, for the differentiation, migration and survival of GCPs, thus indicating that Btg1 plays a role in the development of the cerebellum. Such a role is in cooperation with Tis21 and is consistent with the strong expression of Btg1 observed in the EGL at P7 (Farioli-Vecchioli et al., 2014b).

#### 4.1. The ablation of Btg1 causes hyperproliferation of GCPs and expansion of the EGL during the cerebellar development

The proliferation of the GCPs at the surface of the EGL (outer EGL) is driven by Shh and is maximal 1 week after birth, but after 3 weeks GCPs have differentiated and migrated inward from the EGL to their final destination, i.e., the internal granular layer (IGL; Hatten, 1999). Thus, at P14 the EGL thickness is greatly reduced, to only few layers of GCPs (Fujita et al., 1966). Therefore, it is surprising that following ablation of Btg1 the proliferation in the EGL is still high at P14 and is associated to a several layers-thick EGL. Furthermore, in Btg1-null mice we observed a decrease of

differentiation and migration of GCPs out of the EGL. We should consider that differentiation and migration are correlated, since differentiation can occur only after GCPs have migrated outside the proliferative EGL region controlled by the strong mitogen Shh (Choi et al., 2005). Thus, an explanation of the increased thickness of the EGL may lie not only in the increased cell cycle activity and expansion of the GCPs lacking the antiproliferative gene Btg1, but also in the decrease of migration from the EGL observed at P9 and P16. This effect, however, appears to be non-intrinsic to the Btg1-null GCP, as we show in the in vitro migration analysis of isolated GCPs.

Nevertheless, at P19 the EGL thickness is reduced to a monolayer of GCPs in both Btg1-null and wild-type mice; moreover, 2 months after birth the EGL of Btg1 knockout mice has disappeared as in normal conditions, but the cerebellar volume is greater than in the wild-type. This suggests that the Btg1-null GCP undergoes a transient increase of proliferation rate with consequent increase of EGL size, still detectable at P14, which may also be favored by the concomitant secondary decrease of migration of GCPs from the EGL. However, the GCPs within the hyperplastic EGL of Btg1-null mice undergo continued apoptosis and, importantly, they continue to migrate although with a reduced rate, even when the process of migration in normal mice has almost ceased (at P19). This process tends towards a gradual disappearance of the EGL region, but is not sufficient to regain a normal cerebellar volume in the adult Btg1-null mice. Notably, moreover, the motor coordination, indicative of the cerebellar function, is heavily impaired; this may be linked to the hyperproliferation of the GCPs observed during development, which may permanently affect the cerebellar circuitry and the ability to correctly integrate the sensory input. So far, we know of only one other example of extensive proliferation of the GCPs associated to neuromotor deficit, i.e., the prion protein knockout mouse (Prestori et al., 2008).

Overall, the primary defect of the Btg1-null GCPs is the lack of cell cycle control, while the deficit of differentiation and migration, being quantitatively lower, seem secondary effects. In fact, the deficit of migration in Btg1-null GCPs is rather dependent on the higher proliferation and expansion of GCPs that prevents the normal occurrence of the correlated processes of differentiation and migration, since differentiation is incompatible with a sustained proliferation (Artegiani et al., 2011).

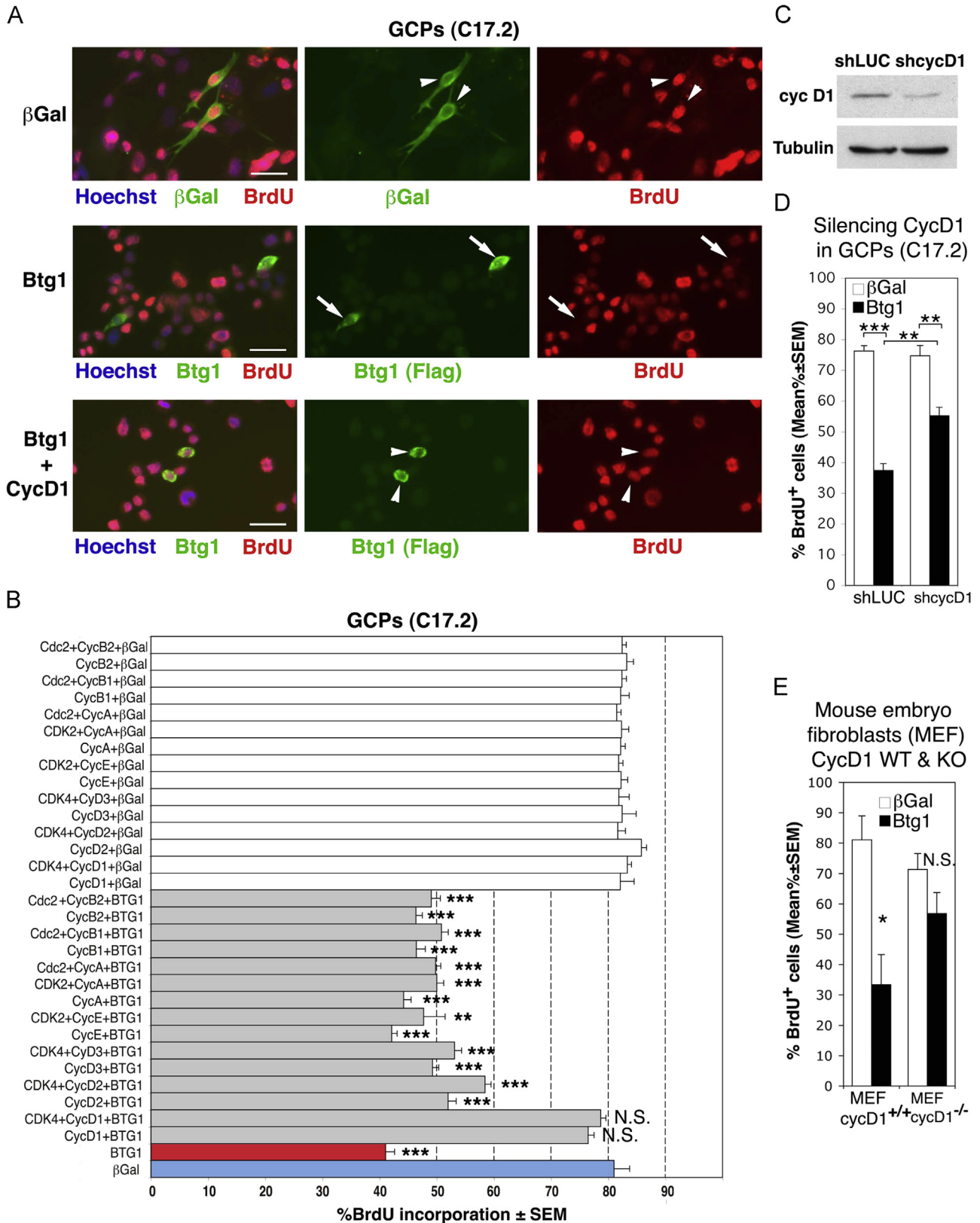
The knockout of Tis21, in comparison, causes a major cell-intrinsic deficit of migration of GCPs from the EGL at P9, still detectable at P12, without effect on proliferation (Farioli-Vecchioli et al., 2012a, and present data). Since, however, Tis21 overexpressed in GCPs strongly inhibits their proliferation (Farioli-Vecchioli et al., 2007), it is probable that in Tis21-null mice Btg1 substitutes for the antiproliferative action of Tis21, up to a plateau. The defective motor coordination in Tis21-null mice might be essentially dependent on the altered process of migration, which is critical for the timing of differentiation of the GCPs and thus for their function.

We also obtain evidence that the development of the cerebellum requires the concomitant action of Btg1 and Tis21. In fact, most remarkably, double mutants Btg1<sup>-/-</sup>/Tis21<sup>-/-</sup> exhibit permanent changes of adult cerebellar morphology more marked than in single mutants (increased area of both ML and IGL layers and cerebellar volume), evidently resulting from the combination of the two major defects of Btg1-null and Tis21-null cerebella, i.e., increased proliferation and highly reduced migration of the GCPs, respectively. A possible explanation is that a longer permanence of the GCPs inside a more actively proliferating EGL area may protract the generation of the GCPs, resulting in a cerebellum of greater size, which also shows the most severe and steady impairments of motor coordination throughout the whole test.

Nevertheless, it is worth noting that the proliferation rate and migration of double mutant GCPs are equivalent to those observed in single *Btg1* or *Tis21* mutant, respectively, which suggest that no evident interference between cellular phenotypes takes place.

#### 4.2. *Btg1*-dependent control of cell cycle by cyclin D1 in GCPs

Notably, we observe that in the *Btg1*-null EGL the number of GCPs expressing cyclin D1 increases significantly, whereas no



change in the expression of cyclin D2 or cyclin A takes place.

Indeed, it is known that Btg1 inhibits cellular proliferation (Rouault et al., 1992; Rodier et al., 1999) by regulating the S-phase of the cell cycle (Farioli-Vecchioli et al., 2014b; Li et al., 2009). It has been shown, however, that in breast cancer cells the action of Btg1 on the G1-S phase of cell cycle involves not only cyclin D1 but also, paradoxically, cyclin B1 (Zhu et al. 2013). In contrast, our data in GCPs within the EGL or in vitro show a preferential, if not exclusive, role for cyclin D1 in the inhibitory control of the cell cycle exerted by Btg1. This would indicate that in normal neural and non-neural cells whose G1-S checkpoint is intact (i.e., unlike in cancer cells), the negative regulation of the cell cycle by Btg1 is exerted mainly by cyclin D1. This finding has an important functional correlate, as cyclin D1 controls the restriction point, i.e., the decisional step whether to enter or not the cell cycle (Sherr and Roberts, 1995). Notably, cyclin D1 is essential for cerebellar development, since cyclin D1-null cerebella fail to attain normal size and morphology in consequence of reduced GCPs proliferation (Pogoriler et al., 2006). Therefore, the finding of a cyclin D1-dependent control of cell cycle further points to a role of Btg1 in the control of proliferation of precursor cells in the cerebellum, fully in line with our recent findings indicating that Btg1 controls the proliferation and quiescence of stem cells in the dentate gyrus and subventricular zone (Farioli-Vecchioli et al., 2014b, 2012c).

A partially similar situation has been observed for Tis21, which regulates the G1/S transition by controlling cyclin D1 expression in normal cells, or by controlling cyclin E expression in tumor cells devoid of pRb (Guardavaccaro et al., 2000; Lim et al., 1998), but also indirectly regulates the G2/M phase in DNA-damaged or in tumor cells, which are defective for the G1-S checkpoint (Tirone, 2001; Rouault et al., 1996; Sundaramoorthy et al., 2013).

Remarkably, the ablation of Btg1 induces in early postnatal dentate gyrus progenitor cells (at P7) an initial strong increase of proliferation, exactly as observed in cerebellum for GCPs; however, in adult mice (at P60) the proliferation of Btg1-null neural stem cells becomes lower than in wild-type mice, with an increased exit from cell cycle and loss of proliferative capacity (Farioli-Vecchioli et al., 2012c). We can speculate that such age-dependent loss of proliferative capacity is not observed in Btg1-null cerebellar precursors only because they do not continue to proliferate during adulthood, as occurs in the dentate gyrus or in the subventricular zone, but cease dividing at an early postnatal age.

As the ablation of Tis21 does not affect cyclin D1 levels in the cerebellum (Farioli-Vecchioli et al., 2012a), it will be interesting to investigate the mechanism underlying the regulation of cyclin D1 by Btg1. In fact, the different functions expressed by Tis21 and Btg1 on cerebellar development may depend on the different availability or activity of partner proteins in the cerebellum. It is known that both Tis21 and Btg1 bind the histone modifying factor Prmt1 (Lin et al., 1996), the transcription factor HoxB9 (Prévôt et al.,

2000), the differentiative receptor RAR $\alpha$  (Passeri et al., 2006), and the transcriptional element Caf1 (Prévôt et al., 2001). Tis21 binds also Smad1 (Park et al., 2004), and the histone deacetylases HDAC1 and HDAC4 (Farioli-Vecchioli et al., 2007), but it is unknown whether these bind Btg1 (see Winkler, 2010). Since all these regulatory proteins are expressed in the cerebellum (Tong and Kwan, 2013; Yoo et al., 2013; Price et al., 2013; GeneCards or BioGPS databases), a possibility to be tested is whether Smad1, HDAC1 or HDAC4 underlie the differential control of Tis21 versus Btg1 in the cerebellum. A further possibility would entail a differential phosphorylation of Tis21 vs Btg1 in the cerebellum, e.g., by CDK2 at serine 147 of Tis21, through which it has been shown to modulate cell proliferation (Guardavaccaro et al., 2000), or at the equivalent serine 159 of Btg1 (Bogdan et al., 1998); or, again a phosphorylation at serine 147 and 159, respectively, by Erk1/2 (Hong et al., 2005).

In conclusion, our data indicate that Btg1 is required for the development and function of the cerebellum, by acting essentially as a regulator of the proliferation of GCPs through inhibition of cyclin D1. Nevertheless, we cannot exclude an intrinsic action of Btg1 also on the differentiation of the GCP. This profile of action of Btg1 on the GCPs maturation based on the control of proliferation is opposite to the profile observed for the highly homologous family-related gene Tis21, whose ablation does not affect the proliferation but rather impairs the intrinsic ability to migrate of GCPs. Moreover, the maturation of the GCPs within the EGL and then through their route to the inner layers requires the actions of both Btg1 and Tis21. Without these, the development of the cerebellum presents permanent morphological defects, with an adult cerebellum significantly larger, and defects in motor coordination.

Considering the hyperplastic EGL observed in Btg1-null mice and the inhibition exerted by Btg1 on the proliferation of medulloblastoma cells, future studies, using mouse models of spontaneous medulloblastoma crossed to Btg1 knockout mice, will be required to ascertain whether Btg1 may play a part in the tumorigenesis of cerebellum.

## Acknowledgments

This work was supported by grants from the Italian Ministry of Economy and Finance to CNR (Project FaReBio; to F.Tirone). M. Ceccarelli is recipient of fellowships from the Italian Foundation for Cancer Research (FIRC; year 2014) and from Fondazione Santa Lucia (year 2015). A patent was filed by the National Research Council on the possible use of the chemokine Cxcl3 in medulloblastoma therapy.

**Fig. 10.** Specific rescue by cyclin D1 of the Btg1-dependent G1 arrest. (A) Representative immunofluorescence photomicrographs of BrdU incorporation in C17.2 cells (GCPs) overexpressing Btg1  $\pm$  cyclin D1, or control  $\beta$ Gal. White arrows and arrowheads: BrdU-negative or BrdU-positive cells, respectively (either Btg1<sup>+</sup> or  $\beta$ -Gal<sup>+</sup>). Nuclei were detected by Hoechst 33258 dye. Bar, 34  $\mu$ m. (B) Percentage of BrdU<sup>+</sup> C17.2 cells after transfection with pSCT- $\beta$ Gal (white bars) or with pSCT-HA-FLAG-Btg1 (red and grey bars). C17.2 cells ( $1 \times 10^5$ ) were seeded onto 35-mm-diameter dishes. After 24 h, cells were transfected with the expression vector pSCT-HA-FLAG-Btg1 (Btg1, 0.4  $\mu$ g) or pSCT- $\beta$ Gal ( $\beta$ Gal, 0.4  $\mu$ g), together with the indicated cyclins (0.8  $\mu$ g) and CDKs (0.8  $\mu$ g). In transfections where the CDK or the cyclin was not present, a corresponding amount (0.8  $\mu$ g) of the empty CMV vector was cotransfected. To measure proliferating cells (BrdU<sup>+</sup>) 50  $\mu$ M BrdU was added to the culture medium 40 h after transfection and cells were fixed after 18 h. Btg1 was detected by anti-Flag antibody (green). Values are calculated as the percentage ratio of BrdU<sup>+</sup> $\beta$ Gal<sup>+</sup> or BrdU<sup>+</sup>Btg1-Flag<sup>+</sup> cells to the total number of  $\beta$ Gal<sup>+</sup> or Btg1-Flag<sup>+</sup> cells, respectively. The results are means  $\pm$  SEM of at least three independent experiments. At least 30 cells were scored for each experiment. \*\*  $p < 0.01$  vs  $\beta$ Gal; \*\*\*  $p \leq 0.001$  vs  $\beta$ Gal; N.S.,  $p > 0.05$  vs  $\beta$ Gal (Student's *t* test). (C,D,E) Requirement of cyclin D1 for the inhibition of G1-S progression by Btg1. (C) Analysis of cyclin D1 protein expression in C17.2 cells, stably infected with retroviruses generated by the pSUPER.retro-puro-shcycD1 or pSUPER.retro-puro-shLUC vectors (see Methods). (D) C17.2 cells stably infected with shCycD1 or shLUC retroviruses, or (E) cyclin D1<sup>+/+</sup> and cyclin D1<sup>-/-</sup> MEF cells, were seeded in 35-mm-diameter dishes and transfected after 24 h with the expression vector pSCT- $\beta$ Gal or pSCT-HA-FLAG-Btg1 (1.5  $\mu$ g each). DNA synthesis assays were performed by adding 50  $\mu$ M BrdU to the culture medium either 48 or 36 h after transfection (for C17.2 or MEF cells, respectively). 18 or 24 h later (for C17.2 or MEF cells, respectively), cells were fixed, permeabilized, and stained. Values are calculated as the percentage ratio of BrdU<sup>+</sup> $\beta$ Gal<sup>+</sup> or BrdU<sup>+</sup>Btg1-Flag<sup>+</sup> cells to the total number of  $\beta$ Gal<sup>+</sup> or Btg1-Flag<sup>+</sup> cells, respectively. Means  $\pm$  SEM are from three independent experiments. At least 70 cells for each group were counted. \*  $p < 0.05$ , \*\*  $p < 0.01$  or \*\*\*  $p < 0.001$  vs control group, Student's *t* test.

## Appendix A. Supplementary material

Supplementary data associated with this article can be found in the online version at <http://dx.doi.org/10.1016/j.ydbio.2015.10.007>.

## References

- Alder, J., Cho, N., Hatten, M., 1996. Embryonic precursor cells from the rhombic lip are specified to a cerebellar granule neuron identity. *Neuron* 17, 389–399.
- Alder, J., Lee, K.J., Jessell, T.M., Hatten, M.E., 1999. Generation of cerebellar granule neurons in vivo by transplantation of BMP-treated neural progenitor cells. *Nat. Neurosci.* 2, 535–540.
- Artegiani, B., Lindemann, D., Calegari, F., 2011. Overexpression of cdk4 and cyclinD1 triggers greater expansion of neural stem cells in the adult mouse brain. *J. Exp. Med.* 208, 937–948.
- Baumann, K., 2013. Cell cycle: cyclin A corrections. *Nat. Rev. Mol. Cell. Biol.* 14, 692.
- Ben-Arie, N., Bellen, H.J., Armstrong, D.L., McCall, A.E., Gordadze, P.R., Guo, Q., Matzuk, M.M., Zoghbi, H.Y., 1997. Math1 is essential for genesis of cerebellar granule neurons. *Nature* 390, 169–172.
- Bogdan, J.A., Adams-Burton, C., Pedicord, D.L., Sukovich, D.A., Benfield, P.A., Corjay, M.H., Stoltenberg, J.K., Dicker, I.B., 1998. Human carbon catabolite repressor protein (CCR4)-associative factor 1: cloning, expression and characterization of its interaction with the B-cell translocation protein BTG1. *Biochem. J.* 336, 471–481.
- Boiko, A.D., Porteous, S., Razorenova, O.V., Krivokrysenko, V.I., Williams, B.R., Gudkov, A.V., 2006. A systematic search for downstream mediators of tumor suppressor function of p53 reveals a major role of BTG2 in suppression of Ras-induced transformation. *Genes Dev.* 20, 236–252.
- Bradbury, A., Possenti, R., Shooter, E.M., Tirone, F., 1991. Molecular cloning of PC3, a putatively secreted protein whose mRNA is induced by nerve growth factor and depolarization. *Proc. Natl. Acad. Sci. USA* 88, 3353–3357.
- Canzoniere, D., Farioli-Vecchioli, S., Conti, F., Ciotti, M.T., Tata, A.M., Augusti-Tocco, G., Mattei, E., Lakshmana, M.K., Krizhanovsky, V., Reeves, S.A., Giovannoni, R., Castano, F., Servadio, A., Ben-Arie, N., Tirone, F., 2004. Dual control of neurogenesis by PC3 through cell cycle inhibition and induction of Math1. *J. Neurosci.* 24, 3355–3369.
- Choi, Y., Borghesani, P.R., Chan, J.A., Segal, R.A., 2005. Migration from a mitogenic niche promotes cell-cycle exit. *J. Neurosci.* 25, 10437–10445.
- Crawley, J.N., 1999. Behavioral phenotyping of transgenic and knockout mice: experimental design and evaluation of general health, sensory functions, motor abilities, and specific behavioral tests. *Brain Res.* 835, 18–26.
- Dahmane, N., Ruiz i Altaba, A., 1999. Sonic hedgehog regulates the growth and patterning of the cerebellum. *Development* 126, 3089–3100.
- Evangelisti, C., Astolfi, A., Gaboardi, G.C., Tazzari, P., Pession, A., Goto, K., Martelli, A.M., 2009. TIS21/BTG2/PC3 and cyclin D1 are key determinants of nuclear diacylglycerol kinase-zeta-dependent cell cycle arrest. *Cell. Signal* 21, 801–809.
- Farioli-Vecchioli, S., Ceccarelli, M., Saraulli, D., Micheli, L., Cannas, S., D'Alessandro, F., Scardigli, R., Leonardi, L., Cinà, I., Costanzi, M., Mattered, A., Cestari, V., Tirone, F., 2014a. Tis21 is required for adult neurogenesis in the subventricular zone and for olfactory behavior regulating cyclins, BMP4, Hes1/5 and Ids. *Front. Cell. Neurosci.* 8, 98.
- Farioli-Vecchioli, S., Cinà, I., Ceccarelli, M., Micheli, L., Leonardi, L., Ciotti, M.T., De Bardi, M., Di Rocco, C., Pallini, R., Cavallaro, S., Tirone, F., 2012a. Tis21 knock-out enhances the frequency of medulloblastoma in Patched1 heterozygous mice by inhibiting the Cxcl3-dependent migration of cerebellar neurons. *J. Neurosci.* 32, 15547–15564.
- Farioli-Vecchioli, S., Mattered, A., Micheli, L., Ceccarelli, M., Leonardi, L., Saraulli, D., Costanzi, M., Cestari, V., Rouault, J.-P., Tirone, F., 2014b. Running rescues defective adult neurogenesis by shortening the length of the cell cycle of neural stem and progenitor cells. *Stem Cells* 32, 1968–1982.
- Farioli-Vecchioli, S., Micheli, L., Leonardi, L., Ceccarelli, M., Cavallaro, S., Tirone, F., 2012b. Medulloblastoma or not? Crucial role in tumorigenesis of the timing of migration of cerebellar granule precursor cells, regulated by Nos2 and Tis21. *Front. Neurosci.* 6, 198.
- Farioli-Vecchioli, S., Micheli, L., Saraulli, D., Ceccarelli, M., Cannas, S., Scardigli, R., Leonardi, L., Cinà, I., Costanzi, M., Ciotti, M.T., Moreira, P., Rouault, J.P., Cestari, V., Tirone, F., 2012c. Btg1 is required to maintain the pool of stem and progenitor cells of the dentate gyrus and subventricular zone. *Front. Neurosci.* 6, 124.
- Farioli-Vecchioli, S., Saraulli, D., Costanzi, M., Leonardi, L., Cinà, I., Micheli, L., Nutini, M., Longone, P., Oh, S.P., Cestari, V., Tirone, F., 2009. Impaired terminal differentiation of hippocampal granule neurons and defective contextual memory in PC3/Tis21 knockout mice. *PLoS One* 4, e8339.
- Farioli-Vecchioli, S., Tanori, M., Micheli, L., Mancuso, M., Leonardi, L., Saran, A., Ciotti, M.T., Ferretti, E., Gulino, A., Pazzaglia, S., Tirone, F., 2007. Inhibition of medulloblastoma tumorigenesis by the antiproliferative and pro-differentiative gene PC3. *FASEB J.* 21, 2215–2225.
- Fujita, S., Shimada, M., Nakamura, T., 1966. H3-thymidine autoradiographic studies on the cell proliferation and differentiation in the external and the internal granular layers of the mouse cerebellum. *J. Comp. Neurol.* 128, 191–208.
- Gibson, P., Tong, Y., Robinson, G., Thompson, M.C., Curre, D.S., Eden, C., Kranenburg, T.A., Hogg, T., Poppleton, H., Martin, J., Finkelstein, D., Pounds, S., Weiss, A., Patay, Z., Scoggins, M., Ogg, R., Pei, Y., Yang, Z.J., Brun, S., Lee, Y., Zindy, F., Lindsey, J.C., Taketo, M.M., Boop, F.A., Sanford, R.A., Gajjar, A., Clifford, S.C., Roussel, M.F., McKinnon, P.J., Gutmann, D.H., Ellison, D.W., Wechsler-Reya, R., Gilbertson, R.J., 2010. Subtypes of medulloblastoma have distinct developmental origins. *Nature* 468, 1095–1099.
- Guardavaccaro, D., Corrente, G., Covone, F., Micheli, L., D'Agnano, I., Starace, G., Caruso, M., Tirone, F., 2000. Arrest of G(1)-S progression by the p53-inducible gene PC3 is Rb dependent and relies on the inhibition of cyclin D1 transcription. *Mol. Cell. Biol.* 20, 1797–1815.
- Hatten, M., 1999. Central nervous system neuronal migration. *Annu. Rev. Neurosci.* 22, 511–539.
- Hong, J.W., Ryu, M.S., Lim, I.K., 2005. Phosphorylation of serine 147 of tis21/BTG2/pc3 by p-Erk1/2 induces Pin-1 binding in cytoplasm and cell death. *J. Biol. Chem.* 280, 21256–21263.
- Jacobsen, P.F., Jenkyn, D.J., Papadimitriou, J.M., 1985. Establishment of a human medulloblastoma cell line and its heterotransplantation into nude mice. *J. Neuropathol. Exp. Neurol.* 44, 472–485.
- Kadin, M.E., Rubinstein, L.J., Nelson, J.S., 1970. Neonatal cerebellar medulloblastoma originating from the fetal external granular layer. *J. Neuropathol. Exp. Neurol.* 29, 583–600.
- Kokubo, M., Nishio, M., Ribar, T.J., Anderson, K.A., West, A.E., Means, A.R., 2009. BDNF-mediated cerebellar granule cell development is impaired in mice null for CaMKK2 or CaMKIV. *J. Neurosci.* 29, 8901–8913.
- Li, F., Liu, J., Park, E.S., Jo, M., Curry Jr, T.E., 2009. The B cell translocation gene (BTG) family in the rat ovary: hormonal induction, regulation, and impact on cell cycle kinetics. *Endocrinology* 150, 3894–3902.
- Lim, I.K., Lee, M.S., Ryu, M.S., Park, T.J., Fujiki, H., Eujiki, H., Paik, W.K., 1998. Induction of growth inhibition of 293 cells by downregulation of the cyclin E and cyclin-dependent kinase 4 proteins due to overexpression of TIS21. *Mol. Carcinog.* 23, 25–35.
- Lin, W.J., Gary, J.D., Yang, M.C., Clarke, S., Herschman, H.R., 1996. The mammalian immediate-early TIS21 protein and the leukemia-associated BTG1 protein interact with a protein-arginine N-methyltransferase. *J. Biol. Chem.* 271, 15034–15044.
- Lu, Q., Sun, E.E., Klein, R.S., Flanagan, J.G., 2001. Ephrin-B reverse signaling is mediated by a novel PDZ-RGS protein and selectively inhibits G protein coupled chemoattraction. *Cell* 105, 69–79.
- Lumpkin, E.A., Collisson, T., Parab, P., Omer-Abdalla, A., Haeblerle, H., Chen, P., Doetzlhofer, A., White, P., Groves, A., Segil, N., Johnson, J.E., 2003. Math1-driven GFP expression in the developing nervous system of transgenic mice. *Gene Expr. Patterns* 3, 389–395.
- Marazziti, D., Di Pietro, C., Golini, E., Mandillo, S., La Sala, G., Matteoni, R., Tocchini-Valentini, G.P., 2013. Precocious cerebellum development and improved motor functions in mice lacking the astrocyte cilium-, patched 1-associated Gpr3711 receptor. *Proc. Natl. Acad. Sci. USA* 110, 16486–16491.
- Marino, S., 2005. Medulloblastoma: developmental mechanisms out of control. *Trends Mol. Med.* 11, 17–22.
- Micheli, L., Leonardi, L., Conti, F., Buanne, P., Canu, N., Caruso, M., Tirone, F., 2011. PC4/Tis7/IFRD1 stimulates skeletal muscle regeneration and is involved in myoblast differentiation as a regulator of MyoD and NF-kappaB. *J. Biol. Chem.* 286, 691–707.
- Miyata, T., Maeda, T., Lee, J.E., 1999. NeuroD is required for differentiation of the granule cells in the cerebellum and hippocampus. *Genes Dev.* 13, 1647–1652.
- Montagnoli, A., Guardavaccaro, D., Starace, G., Tirone, F., 1996. Overexpression of the nerve growth factor-inducible PC3 immediate early gene is associated with growth inhibition. *Cell. Growth Differ.* 7, 1327–1336.
- Park, S., Lee, Y.J., Lee, H.J., Seki, T., Hong, K.H., Park, J., Beppu, H., Lim, I.K., Yoon, J.W., Li, E., Kim, S.J., Oh, S.P., 2004. B-cell translocation gene 2 (Btg2) regulates vertebral patterning by modulating bone morphogenetic protein/smud signaling. *Mol. Cell. Biol.* 24, 10256–10262.
- Passeri, D., Marcucci, A., Rizzo, G., Billi, M., Panigada, M., Leonardi, L., Tirone, F., Grignani, F., 2006. Btg2 enhances retinoic acid-induced differentiation by modulating histone H4 methylation and acetylation. *Mol. Cell. Biol.* 26, 5023–5032.
- Pogoriler, J., Millen, K., Utset, M., Du, W., 2006. Loss of cyclin D1 impairs cerebellar development and suppresses medulloblastoma formation. *Development* 133, 3929–3937.
- Prestori, F., Rossi, P., Bearzatto, B., Lainé, J., Necchi, D., Diwakar, S., Schifmann, S.N., Axelrad, H., D'Angelo, E., 2008. Altered neuron excitability and synaptic plasticity in the cerebellar granular layer of juvenile prion protein knock-out mice with impaired motor control. *J. Neurosci.* 28, 7091–7103.
- Prévôt, D., Voeltzel, T., Birot, A.M., Morel, A.P., Rostan, M.C., Magaud, J.P., Corbo, L., 2000. The leukemia-associated protein Btg1 and the p53-regulated protein Btg2 interact with the homeoprotein Hoxb9 and enhance its transcriptional activation. *J. Biol. Chem.* 275, 147–153.
- Prévôt, D., Morel, A.P., Voeltzel, T., Rostan, M.C., Rimokh, R., Magaud, J.P., Corbo, L., 2001. Relationships of the antiproliferative proteins BTG1 and BTG2 with CAF1, the human homolog of a component of the yeast CCR4 transcriptional complex: involvement in estrogen receptor alpha signaling pathway. *J. Biol. Chem.* 276, 9640–9648.
- Price, V., Wang, L., D'Mello, S.R., 2013. Conditional deletion of histone deacetylase-4 in the central nervous system has no major effect on brain architecture or neuronal viability. *J. Neurosci. Res.* 91, 407–415.
- Qiu, Z., Cang, Y., Goff, S.P., 2010. Abl family tyrosine kinases are essential for basement membrane integrity and cortical lamination in the cerebellum. *J. Neurosci.* 30, 14430–14439.
- Rakic, P., 1971. Neuron-glia relationship during granule cell migration in developing

- cerebellar cortex. A golgi and electron microscopy study in *Macacus rhesus*. *J. Comp. Neurol.* 141, 283–312.
- Reeber, S.L., Otis, T.S., Sillitoe, R.V., 2013. New roles for the cerebellum in health and disease. *Front. Syst. Neurosci.* 7, 83.
- Rodier, A., Marchal-Victorion, S., Rochard, P., Casas, F., Cassar-Malek, I., Rouault, J.P., Magaud, J.P., Mason, D.Y., Wrutniak, C., Cabello, G., 1999. BTG1: a triiodothyronine target involved in the myogenic influence of the hormone. *Exp. Cell. Res.* 249, 337–348.
- Rouault, J.P., Falette, N., Guehenneux, F., Guillot, C., Rimokh, R., Wang, Q., Berthet, C., Moyret-Lalle, C., Savatier, P., Pain, B., Shaw, P., Berger, R., Samarut, J., Magaud, J.P., Ozturk, M., Samarut, C., Puisieux, A., 1996. Identification of BTG2, an anti-proliferative p53-dependent component of the DNA damage cellular response pathway. *Nat. Genet.* 14, 482–486.
- Rouault, J.P., Rimokh, R., Tessa, C., Paranhos, G., Ffrench, M., Duret, L., Garocchio, M., Germain, D., Samarut, J., Magaud, J.P., 1992. BTG1, a member of a new family of antiproliferative genes. *EMBO J.* 11, 1663–1670.
- Ryder, E.F., Snyder, E.Y., Cepko, C.L., 1990. Establishment and characterization of multipotent neural cell lines using retrovirus vector-mediated oncogene transfer. *J. Neurobiol.* 21, 356–375.
- Schüller, U., Heine, V.M., Mao, J., Kho, A.T., Dillon, A.K., Han, Y.G., Huillard, E., Sun, T., Ligon, A.H., Qian, Y., Ma, Q., Alvarez-Buylla, A., McMahon, A.P., Rowitch, D.H., Ligon, K.L., 2008. Acquisition of granule neuron precursor identity is a critical determinant of progenitor cell competence to form Shh-induced medulloblastoma. *Cancer Cell.* 14, 123–134.
- Sherr, C.J., Roberts, J.M., 1995. Inhibitors of mammalian G1 cyclin-dependent kinases. *Genes Dev.* 9, 1149–1163.
- Sudarov, A., Joyner, A.L., 2007. Cerebellum morphogenesis: the foliation pattern is orchestrated by multi-cellular anchoring centers. *Neural Dev.* 2, 26.
- Sundaramoorthy, S., Ryu, M.S., Lim, I.K., 2013. B-cell translocation gene 2 mediates crosstalk between PI3K/Akt1 and NFκB pathways which enhances transcription of MNSOD by accelerating IκBα degradation in normal and cancer cells. *Cell. Commun. Signal.* 11, 69.
- Tirone, F., 2001. The gene PC3(TIS21/BTG2), prototype member of the PC3/BTG/TOB family: regulator in control of cell growth, differentiation, and DNA repair? *J. Cell. Physiol.* 187, 155–165.
- Tong, K.K., Kwan, K.M., 2013. Common partner Smad-independent canonical bone morphogenetic protein signaling in the specification process of the anterior rhombic lip during cerebellum development. *Mol. Cell. Biol.* 33, 1925–1937.
- Wallace, V.A., 1999. Purkinje-cell-derived Sonic hedgehog regulates granule neuron precursor cell proliferation in the developing mouse cerebellum. *Curr. Biol.* 9, 445–448.
- Wang, J., Wechsler-Reya, R.J., 2014. The role of stem cells and progenitors in the genesis of medulloblastoma. *Exp. Neurol.* 260, 69–73.
- Wechsler-Reya, R.J., Scott, M.P., 1999. Control of neuronal precursor proliferation in the cerebellum by Sonic hedgehog. *Neuron* 22, 103–114.
- Weyer, A., Schilling, K., 2003. Developmental and cell type-specific expression of the neuronal marker NeuN in the murine cerebellum. *J. Neurosci. Res.* 73, 400–409.
- Wingate, R.J.T., 2001. The rhombic lip and early cerebellar development. *Curr. Opin. Neurobiol.* 11, 82–88.
- Winkler, G.S., 2010. The mammalian anti-proliferative BTG/Tob protein family. *J. Cell. Physiol.* 222, 66–72.
- Yang, Z.J., Ellis, T., Markant, S.L., Read, T.A., Kessler, J.D., Bourbonnas, M., Schüller, U., Machold, R., Fishell, G., Rowitch, D.H., Wainwright, B.J., Wechsler-Reya, R.J., 2008. Medulloblastoma can be initiated by deletion of Patched in lineage-restricted progenitors or stem cells. *Cancer Cell* 14, 135–145.
- Yoo, J.Y., Larouche, M., Goldowitz, D., 2013. The expression of HDAC1 and HDAC2 during cerebellar cortical development. *Cerebellum* 12, 534–546.
- Zhu, R., Zou, S.T., Wan, J.M., Li, W., Li, X.L., Zhu, W., 2013. BTG1 inhibits breast cancer cell growth through induction of cell cycle arrest and apoptosis. *Oncol. Rep.* 30, 2137–2144.